

CORNELL UNIVERSITY MATHEMATICS DEPARTMENT SENIOR THESIS

***Homotopies of Eigenfunctions and the
Spectrum of the Laplacian on the Sierpinski
Carpet***

A THESIS PRESENTED IN PARTIAL FULFILLMENT
OF CRITERIA FOR HONORS IN MATHEMATICS

Steven Michael Heilman

May 2009

BACHELOR OF ARTS, CORNELL UNIVERSITY

THESIS ADVISOR(S)

Robert Strichartz
Department of Mathematics

Homotopies of Eigenfunctions and the Spectrum of the Laplacian on the Sierpinski Carpet

Steven M. Heilman[†] Robert S. Strichartz[‡]

April 19, 2009

Abstract

Consider a family of bounded domains Ω_t in the plane (or more generally any Euclidean space) that depend analytically on the parameter t , and consider the ordinary Neumann Laplacian Δ_t on each of them. Then we can organize all the eigenfunctions into continuous families $u_t^{(j)}$ with eigenvalues $\lambda_t^{(j)}$ also varying continuously with t , although the relative sizes of the eigenvalues will change with t at crossings where $\lambda_t^{(j)} = \lambda_t^{(k)}$. We call these families *homotopies* of eigenfunctions. We study two explicit examples. The first example has Ω_0 equal to a square and Ω_1 equal to a circle; in both cases the eigenfunctions are known explicitly, so our homotopies connect these two explicit families. In the second example we approximate the Sierpinski carpet starting with a square, and we continuously delete subsquares of varying sizes. (Data available in full at www.math.cornell.edu/~smh82)

Keywords: analysis on fractals, Laplacian, eigenfunction, spectrum, Sierpinski Carpet

1 INTRODUCTION

Consider a family of bounded domains Ω_t in the plane (or more generally Euclidean space or a Riemannian manifold) depending on a real parameter t . For each domain we consider the standard Laplacian Δ equipped with Neumann boundary conditions. By a *homotopy of eigenfunctions* we mean a continuous family of eigenfunctions $u_t(x)$ with eigenvalues $\lambda(t)$ (also varying continuously in $t \in \mathbb{R}$).

$$\begin{aligned} -\Delta u_t &= \lambda(t)u_t \text{ on } \Omega_t \\ \partial_n u_t &= 0 \text{ on } \partial\Omega_t \end{aligned} \tag{1}$$

For a reasonable domain Ω_t there is a complete orthonormal basis of eigenfunctions. We do not expect every eigenfunction to belong to a homotopy. If the

Department of Mathematics, Cornell University, Ithaca, NY 14850-4201

E-mail address: smh82@cornell.edu

Department of Mathematics, Cornell University, Ithaca, NY 14850-4201

E-mail address: str@math.cornell.edu

[†]: Research supported by the National Science Foundation through the Research Experiences for Undergraduates Program at Cornell.

[‡]: Research supported in part by the National Science Foundation, grant DMS-0652440.

eigenvalue is simple, then it is easy to see that the (unique up to a constant) eigenfunction does belong to a homotopy for at least a small interval in the parameter t . However, if the eigenspace has higher multiplicity at a fixed value of t , the best we can expect is that there is a special basis of eigenfunctions that belong to a homotopy.

We face the same situation if we consider a continuous family A_t of symmetric $n \times n$ matrices. The eigenvalues depend continuously on t , but the eigenvectors do not necessarily vary continuously. For example, let

$$A_t = \begin{cases} t^3 B_1 & t \geq 0 \\ t^3 B_2 & t < 0 \end{cases} \quad (2)$$

for B_1, B_2 2×2 symmetric matrices with different eigenvectors. One can avoid this pathology by assuming that the derivative with respect to t is nonzero, or that the dependence on t is analytic. However, if $A_t = tB$ where B has distinct eigenvectors, then for $t = 0$, the matrix has eigenspace corresponding to $\lambda = 0$ containing all vectors, whereas only the eigenvectors of B belong to homotopies.

Observe now that the double eigenvalue of A_t at $t = 0$ is unstable under perturbation. More specifically, recall that matrices with multiple eigenvalues, considered as a subspace of $n \times n$ symmetric matrices, have codimension 2. Similarly, those matrices with multiple eigenvalues in $n \times n$ Hermitian matrices have codimension 3. So, for a generic one-parameter family of self-adjoint matrices, multiple eigenvalues are very rare. Moreover, in the self-adjoint case, if two eigenvalues move near each other (say, as t increases), the eigenvalues then repel each other. We can see this from the following equation (derived below as in the article¹ "When are eigenvalues stable?"):

$$\lambda_k'' = u_k^* A_t'' u_k + 2 \sum_{j \neq k} \frac{|u_k^* A_t' u_j|}{\lambda_k - \lambda_j} \quad (3)$$

where u_k is the k^{th} eigenfunction (an L^2 normalized column vector), λ_j is the j^{th} eigenvalue, $*$ denotes complex transpose, and $'$ denotes a derivative in the t variable. Note that the eigenvectors and eigenvalues are functions of t .

To obtain Eq. (3), we differentiate the equation $A_t u_k(t) = \lambda_k(t) u_k(t)$ in the t variable to get

$$A_t u_k' + A_t' u_k = \lambda_k u_k' + \lambda_k' u_k \quad (4)$$

We then differentiate the identity $u_k^* u_k = 1$ to get $u_k^* u_k' = 0$. Then, applying u_k^* to both sides of Eq. (4) and using the previous sentence gives

$$\lambda_k' = u_k^* A_t' u_k \quad (5)$$

Notice we have also used the fact that

$$u_k^* A_t = \lambda_k u_k^*, \quad (6)$$

which is just the eigenvalue equation for u_k with the adjoint taken on both sides. Now, apply u_j^* to both sides of Eq. (4) for $j \neq k$, and apply Eq. (6) and the orthogonality of the eigenvectors to the result to obtain

$$u_j^* A_t' u_k + (\lambda_j - \lambda_k) u_j^* u_k' = 0. \quad (7)$$

So, re-writing, summing over j , using the completeness of the eigenvectors (and recalling that $u_j^* u_j' = 0$) gives

$$u_k' = \sum_{j \neq k} \frac{u_j^* A_t' u_k}{\lambda_k - \lambda_j} \quad (8)$$

Now, differentiating Eq. (5) gives

$$\lambda_k'' = u_k^* A_t'' u_k + u_k^* A_t' u_k' + (u_k^*)' A_t' u_k \quad (9)$$

And after applying Eq. (8) to Eq. (9), we finally get Eq. (3).

We now wish to comment further on the significance of Eq. (3). The repulsion of two distinct eigenvalues, or level repulsion, manifests in the second term on the right of Eq. (3). That is, if we increase t linearly, and two eigenvalues λ_k and $\lambda_{k'}$ move close together, the second term of Eq. (3) becomes very large (assuming the numerator does not vanish). In fact, λ_k'' has a term of the form $1/(\lambda_k - \lambda_{k'})$, while $\lambda_{k'}''$ has a term of the form $1/(\lambda_{k'} - \lambda_k)$. So, the larger of the two eigenvalues is forced upward, and the smaller of the two is forced downward. Therefore, Eq. (3) accounts for generic eigenvalue repulsion, in this finite dimensional case.

Now, can these observations carry over to the infinite dimensional setting? We are concerned here with eigenvalue repulsion and rarity of multiple eigenvalues. Specifically, do these effects occur for compact planar domains which vary with a time parameter? To a certain extent, yes. Restricting an infinite dimensional operator to finitely many dimensions as in Eq. (12) below, the repulsion effects from the finite dimensional Hermitian case should carry over to self-adjoint operators. (For rigorous results on the rarity of multiple eigenvalues, see the references^{2, 3, 4}.)

Mimicking the finite dimensional case, we reformulate our original problem by taking a fixed domain Ω and varying the differential operator. We assume that we have a family of diffeomorphisms $\Psi_t : \Omega \rightarrow \Omega_t$ that depends analytically on the parameter t . Then we can pull back the Euclidean metric on Ω_t to a Riemannian metric on Ω . The pullback of the standard Laplacian on Ω_t becomes the Laplace-Beltrami operator on Ω , which we denote by Δ_t . Similarly, we can pull back the energy and measure on Ω_t to the corresponding quantities on Ω for the Riemannian metric. We note that the Neumann boundary conditions correspond, and also the coefficients of Δ_t are analytic functions in t . Let $[a, b]$ be any finite interval in $[0, \infty)$ such that the endpoints are not Neumann eigenvalues of any Δ_t (to do this we may have to restrict the interval in which t varies). Then the spectral projection operator $P_t([a, b])$ associated with $-\Delta_t$ and the interval $[a, b]$ is well-defined and of finite rank, and may be expressed as a contour integral in the resolvent

$$R(\lambda) = \int_{\Gamma} (\lambda + \Delta_t)^{-1} d\lambda \quad (10)$$

for a suitable contour Γ in the complex plane enclosing the interval. The resolvent depends analytically on t (this may be seen via the pseudodifferential calculus, for example), so the projection operator also depends analytically on t . If the rank of the projection operator is N , we can find an N -dimensional

space V of functions such that $P_t([a, b])$ maps V onto its range. Let $P_t^{-1}([a, b])$ denote the inverse. Then we can transform the eigenvalue equation

$$-\Delta_t u_t = \lambda(t)u_t \text{ on } \Omega \quad (11)$$

into the eigenvalue equation

$$-(P_t([a, b])^{-1}\Delta_t P_t([a, b]))x_t = \lambda(t)x_t \text{ in } V \quad (12)$$

via $x_t = P_t([a, b])^{-1}u_t$. Now we are in the finite dimensional setting with a family of operators depending analytically on the parameter, so N homotopies of eigenfunctions exist, and these yield N homotopies of eigenfunctions u_t on Ω .

Once we have the existence of homotopies for small intervals of the parameter and bounded regions of the spectrum, we can combine them to obtain global homotopies for the whole spectrum. If u_{t_0} is an eigenfunction corresponding to a simple eigenvalue $\lambda(t_0)$ of Δ_{t_0} , then there is a unique homotopy u_t with $u_t|_{t=t_0} = u_{t_0}$. If $\lambda(t_0)$ is an eigenvalue of Δ_{t_0} with nontrivial multiplicity, then its eigenspace $E(t_0)$ has a basis of eigenvectors which lie in homotopies. In fact one can take this basis to be orthonormal. Suppose for example, that $\lambda(t_0)$ has multiplicity 2, and let $u_t^{(1)}$ and $u_t^{(2)}$ denote 2 homotopies with eigenvalues $\lambda^{(1)}(t)$ and $\lambda^{(2)}(t)$. Then either $\lambda^{(1)}(t) = \lambda^{(2)}(t)$ for all t or $\lambda^{(1)}(t) \neq \lambda^{(2)}(t)$ for $0 < |t - t_0| < \epsilon$. In the first case we may take linear combinations of $u_t^{(1)}$ and $u_t^{(2)}$ to obtain orthogonality. In the second case we have the orthogonality of $u_t^{(1)}$ and $u_t^{(2)}$ for $0 < |t - t_0| < \epsilon$ (because the eigenvalues are distinct), and by continuity it must hold for $t = t_0$.

The deeper question, however, is what is the significance of the homotopies? If we have homotopies between domains Ω_0 and Ω_1 then we have a pairing up of the eigenfunctions on Ω_0 and Ω_1 . What does this tell us about the paired eigenfunctions? The goal of this paper is to investigate this question experimentally. We examine two different examples. In the first, something of a warmup exercise, we take Ω_0 be a circle and Ω_1 to be a square. We know exactly what the eigenfunctions are at both endpoints. For the unit circle, using polar coordinates, the eigenspaces typically have multiplicity 2 and are spanned by $J_m(\lambda_{mk}r) \cos m\theta$ and $J_m(\lambda_{mk}r) \sin m\theta$ where the eigenvalues λ_{mk} are the successive zeroes of J'_m , indexed by $k = 1, 2, 3, \dots$. Here $m = 1, 2, 3, \dots$. The exceptional case $m = 0$ yields a 1-dimensional eigenspace spanned by $J_0(\lambda_{0k}r)$. For the unit square, there is a basis of eigenfunctions of the form $\cos \pi jx \cos \pi ky$ for $j = 0, 1, 2, \dots$ and $k = 0, 1, 2, \dots$ with eigenvalues $\pi^2(j^2 + k^2)$. Typical eigenspaces have dimension 1 ($j = k$) or 2 ($j \neq k$), but higher multiplicity may occur due to coincidences, such as $3^2 + 4^2 = 5^2 + 0^2$ or $7^2 + 1^2 = 5^2 + 5^2$.

In order to simplify and clarify the discussion we consider the action of the dihedral symmetry group D_4 on the eigenspaces. D_4 acts on the circle and square and all the domains we consider. It is well known that this 8 element group has 5 irreducible representations, one being 2-dimensional and the others 1-dimensional. Each eigenspace either transforms according to one of these representations or splits into a direct sum of such pieces, and the homotopies respect the representation types. We denote the 1-dimensional representations $1++$, $1+-$, $1-+$, and $1--$, where the first \pm refers to the symmetry or skew-symmetry with respect to diagonal reflections, and the second \pm refers to the

symmetry or skew-symmetry with respect to horizontal and vertical reflections. We now describe the eigenspaces sorted according to representation type for the circle and the square.

Circle:

- 1 + + : The eigenspace $E_{++}^c(4m, k)$ is generated by $J_{4m}(\lambda_{(4m)k}r) \cos 4m\theta$ for $m = 0, 1, 2, \dots$ and $k = 1, 2, 3, \dots$
- 1 - + : The eigenspace $E_{-+}^c(4m, k)$ is generated by $J_{4m}(\lambda_{(4m)k}r) \sin 4m\theta$ for $m = 1, 2, 3, \dots$ and $k = 1, 2, 3, \dots$
- 1 + - : The eigenspace $E_{+-}^c(4m + 2, k)$ is generated by $J_{4m+2}(\lambda_{(4m+2)k}r) \cos(4m + 2)\theta$ for $m = 0, 1, 2, \dots$ and $k = 1, 2, 3, \dots$
- 1 - - : The eigenspace $E_{--}^c(4m + 2, k)$ is generated by $J_{4m+2}(\lambda_{(4m+2)k}r) \sin(4m + 2)\theta$ for $m = 0, 1, 2, \dots$ and $k = 1, 2, 3, \dots$
- 2 : The eigenspace $E_2^c(2m + 1, k)$ is generated by $J_{2m+1}(\lambda_{(2m+1)k}r) \cos(2m + 1)\theta$ and $J_{2m+1}(\lambda_{(2m+1)k}r) \sin(2m + 1)\theta$ for $m = 0, 1, 2, \dots$ and $k = 1, 2, 3, \dots$

Square:

- 1 + + : The eigenspace $E_{++}^s(2j, 2k)$ is generated by $\cos \pi 2jx \cos \pi 2ky + \cos \pi 2kx \cos \pi 2jy$ for $0 \leq j \leq k$
- 1 - + : The eigenspace $E_{-+}^s(2j, 2k)$ is generated by $\cos \pi 2jx \cos \pi 2ky - \cos \pi 2kx \cos \pi 2jy$ for $0 \leq j < k$
- 1 + - : The eigenspace $E_{+-}^s(2j + 1, 2k + 1)$ is generated by $\cos \pi(2j + 1)x \cos \pi(2k + 1)y + \cos \pi(2k + 1)x \cos \pi(2j + 1)y$ for $0 \leq j \leq k$
- 1 - - : The eigenspace $E_{--}^s(2j + 1, 2k + 1)$ is generated by $\cos \pi(2j + 1)x \cos \pi(2k + 1)y - \cos \pi(2k + 1)x \cos \pi(2j + 1)y$ for $0 \leq j < k$
- 2 : The 2-dimensional eigenspace $E_2^s(2j + 1, 2k)$ is generated by $\cos \pi(2j + 1)x \cos \pi 2ky$ and $\cos \pi 2kx \cos \pi(2j + 1)y$ for $0 \leq j \leq k$

In the case of the square, because of coincidences, the full eigenspace associated with a given eigenvalue may be a direct sum of some of the spaces described above, for example $E_2^s(5, 0) \oplus E_2^s(3, 4)$ or $E_{+-}^s(5, 5) \oplus E_{+-}^s(7, 1)$. When we construct homotopies, we often find that they do not pass through the individual summands. This problem does not arise for the circle, since as far as we know there are no coincidences among the eigenvalues λ_{mk} .

In section 2 we describe the homotopies of eigenfunctions for two different analytic families of domains joining the circle to a square. In one, the circle expands out to a square in horizontal/vertical orientation, and in the other the circle contracts in to a square in diagonal orientation. (The fact that these are not unit squares just requires a trivial adjustment.) In both cases the homotopies connect the same E^s and E^c eigenspaces. We observe a canonical splitting of two-dimensional eigenspaces at the endpoints of the homotopy. We also do not find any two-dimensional eigenspaces away from the endpoints of the homotopy.

In our second example in section 3 we consider a sequence of domains A_i that approximate the Sierpinski carpet (SC). Let F_1, \dots, F_8 denote the similarities that map to square A_0 into the squares of the ‘‘picture frame’’ A_1 that is A_0 with the middle ninth removed. Then

$$SC = \cup_{i=1}^8 F_i(SC) \tag{13}$$

and

$$A_j = \cup_{i=1}^8 F_i(A_{j-1}) \tag{14}$$

In a previous work⁵ we gave experimental evidence that the spectra of the Neumann Laplacians on A_j converge, after the appropriate renormalization, to the spectrum of the Neumann Laplacian on SC , with the eigenfunctions also converging. In other words, there is a complete orthonormal basis $u_n^{(j)}$ of eigenfunctions

$$-\Delta u_n^{(j)} = \lambda_n^{(j)} u_n^{(j)} \quad (15)$$

on A_j with Neumann boundary conditions such that

$$\lim_{j \rightarrow \infty} r^j \lambda_n^{(j)} = \lambda_n \text{ and} \quad (16)$$

$$\lim_{j \rightarrow \infty} u_n^{(j)}|_{SC} = u_n \quad (17)$$

for some $r \in \mathbb{R}$. We would then identify u_n as the Neumann eigenfunctions of the Barlow-Bass⁶ Laplacian Δ on SC . The recently announced proof⁷ of the uniqueness of that Laplacian justifies this identification. Combining this uniqueness result, the resolvent convergence⁸ (see §7), and the relation $e^{t\Delta} f(x) = E_x[f(X_t)]$ between the Laplacian Δ and Brownian motion X_t , suggest a method of rigorous proof of Eq. (17). The relation $e^{t\Delta} f(x) = E_x[f(X_t)]$ is important because it shows that the speeding up of the Brownian motion⁸ exactly corresponds to multiplication of Δ by a constant.

However, even with convergence in Eq. (17), there is an obstacle to uncovering the dynamics of the eigenvalues and eigenfunctions. It was noted⁵ that, for a given n , the eigenvalues $\{\lambda_n^{(j)}\}$ are not necessarily in increasing order (with respect to the original ordering for $j = 0$). In order to better understand the discrete sequence $u_n^{(j)}$ of eigenfunctions, we embed them in homotopies. For example, to connect the square A_0 with the picture frame A_1 , we first remove the center of the square. Since points have zero capacity in the square, this does not change the Neumann Laplacian. We then gradually enlarge the hole by deleting squares in the center with side length going from 0 to $1/3$. Similarly, to go from A_1 to A_2 we enlarge 8 holes in the center of the squares $F_i A_0$ with side length going from 0 to $1/9$. We carried out the computation of these homotopies up to A_4 . (Note that it would also be possible to do a single deformation from A_0 to A_4 by opening all holes simultaneously.) Some eigenfunctions change only slightly during the course of the homotopy; we could say that they make minor adjustments to the changing domains. However, most eigenfunctions show considerable variation, especially for higher eigenvalues. Ideally we would hope to make a reasonable guess from the shape of $u_n^{(4)}$ as to which $u_n^{(0)}$ it is connected to. We are very far from being able to do this. In fact, the following cautionary tale shows some of the obstacles. If j and k are divisible by 3, then all the eigenfunctions in any of the $E^s(j, k)$ spaces are also Neumann eigenfunctions on A_1 (when restricted to A_1). However, many of the homotopies do not connect the restriction to A_1 with the original eigenfunction on A_0 .

2 CIRCLE to SQUARE HOMOTOPY

Let $L \subset \mathbb{R}^2$ denote the line $x + y = 1$ in the closed first quadrant. In polar coordinates L is parameterized by the equation $r = 1/(\cos \theta + \sin \theta)$, $\theta \in [0, \pi/2]$. Then, the map $\psi(r, \theta) = (1/(\cos \theta + \sin \theta)r, \theta)$ defined in the closed first quadrant

takes the arc of the circle of radius 1 centered at the origin to the line L . In fact, it also maps the arc of the circle of radius r to the line $\{(x, y) : x + y = r\}$. With this in mind, let $H(t, r, \theta) : [0, 1] \times \mathbb{R}^2 \rightarrow \mathbb{R}^2$ be the homotopy

$$H(t, r, \theta) = \left(\left((1-t) + \frac{t}{\cos \theta + \sin \theta} \right) r, \theta \right) \quad (18)$$

For $\theta \in [0, \pi/2]$, this is the straight-line homotopy between the identity map of \mathbb{R}^2 and $\psi(r, \theta)$. So, as we vary t , H restricted to the closed first quadrant maps the square diamond of side length $\sqrt{2}$ to the unit disc. Observe that for $t \in (0, 1)$, H (with the same restriction) maps the square to a half-ellipse.

Rotating the domain and range of the map into all four quadrants, we get a straight-line homotopy which connects the square diamond to the unit disc and which is analytic in the time parameter t on $(0, 1)$ (and continuous on $[0, 1]$). If we view $H(t, r, \theta)$ as an analytic deformation of the standard metric on the unit disc, the Neumann Laplacian Δ_t on the disc is a holomorphic family of type (A) (see the reference⁹). Then, Theorem 3.9, VII. §4.5 from the same book says the eigenvalues and eigenvectors can be represented as functions holomorphic in t . More specifically, the eigenvalues are holomorphic functions and the eigenfunctions can be chosen to be holomorphic with a Banach space as their range. In our terminology, we have an (analytic) homotopy of eigenfunctions. This is the theoretical basis of our investigation.

An analogous process can be achieved for $\phi(r, \theta) = (\sqrt{2}/(\cos \theta + \sin \theta)r, \theta)$ and

$$F(t, r, \theta) = \left(\left((1-t) + \frac{\sqrt{2}t}{\cos \theta + \sin \theta} \right) r, \theta \right) \quad (19)$$

where ϕ maps the unit circle in the first quadrant to the square diamond of side length 2, and upon reflection as above, F gives a straight line homotopy between the identity map on the unit circle and $\phi(r, \theta)$. Again, we get a straight-line homotopy from the unit disc to the square, and with previously mentioned results⁹, we have a homotopy of eigenfunctions. Note that F and H are not identical.

Since all of our domains are invariant under the D_4 symmetry group, we can simplify the eigenfunction computations by reducing to a fundamental domain. On this domain we impose appropriate boundary conditions according to the representation type. For the 1-dimensional representation, we restrict to the sector $0 \leq \theta \leq \pi/4$. Recall that the functions will extend evenly when reflected about $\theta = 0$ in the $1++$ and $1-+$ cases, and oddly in the $1+-$ and $1--$ cases. When reflecting about $\theta = \pi/4$, the functions will extend evenly in the $1++$ and $1+-$ cases, and oddly in the $1-+$ and $1--$ cases. Note that performing an even extension across a ray is equivalent to imposing Neumann boundary conditions on that ray. Similarly, the odd extension is equivalent to Dirichlet conditions.

For the 2-dimensional representation our fundamental domain is the sector $0 \leq \theta \leq \pi/2$, and we impose Neumann boundary conditions on the ray $\theta = 0$ and Dirichlet conditions on the ray $\theta = \pi/2$. Notice that our fundamental domains are simply connected. Therefore, as in Theorem 6.4 of Teytel's paper⁴, we should expect no two-dimensional eigenspaces along this homotopy (for each individual symmetry family).

In order for Matlab R2006a to understand our geometry, we must give the geometric data to the program in its desired format. To accomplish this task in Matlab's PDE Toolbox for a fixed t , we specify polygons and circles. More specifically, we specify the vertices of the polygon and the center and radius of a circle, with standard coordinates in the plane. Once we input this data, we then fix a closed interval of the real line in which we look for eigenvalues λ . The program then uses the Arnoldi Algorithm with function `pdeeig` to solve the eigenvalue equation $(-\Delta)u = \lambda u$ for λ in the specified interval. For this particular homotopy, this process yields sixty to seventy eigenvalues within minutes. As our first approximation to a smooth homotopy using H or F , we solve for eigenfunctions at times $t \in \{k/10\}_{k=0}^{10}$. For now, Matlab's solution method is sufficient. However, other solvers based in different programs may be more effective in the future. For instance, the boundary element method appears much more efficient than the finite element method.

In the following diagrams, we show the observed eigenvalue dynamics for each of the five symmetry families $(1++, 1+-, 1-+, 1--, 2)$. For convenience, we divide all eigenvalues by π^2 . As stated above, the data is collected for $t \in \{k/10\}_{k=0}^{10}$. As t varies, we determine whether or not two eigenvalues cross by inference (see below for more details).

Observe that the eigenvalue plots exhibit eigenvalue repulsion, as in Eq. (3) in the finite dimensional setting. When two eigenvalues draw near each other, they "collide" and then veer away rapidly (see Fig. 19 (a) below). Intuitively, when two eigenvalues move near each other, one could imagine a slightly perturbed geometry for which these eigenvalues would be the same. Indeed, the eigenfunctions also support this intuition. If we examine the eigenfunctions before and after the collision, we see that they swap identities. That is, if we have eigenvalues $\lambda_{j+1} > \lambda_j$ which collide around $t = t_0$, then $u_{j+1}(t_0 - \epsilon)$ looks like $u_j(t_0 + \epsilon)$, and $u_j(t_0 - \epsilon)$ looks like $u_{j+1}(t_0 + \epsilon)$. In the intermediate region $(t_0 - \epsilon, t_0 + \epsilon)$, we then observe two linear combinations of our eigenfunctions $u_{j+1}(t_0 - \epsilon)$ and $u_j(t_0 - \epsilon)$. This effect has been observed before¹⁰ and coined the superposition effect. Notice that this superposition effect only occurs among eigenfunctions of the same symmetry class.

When a two-dimensional eigenspace occurs (analytically), the superposition effect is sometimes not observed numerically. For example, consider eigenfunctions u_{13} and u_{14} from the $(1++)$ family on the square. We see from Fig. 1 that these two eigenfunctions separate from the two dimensional eigenspace at $t = 1$, as t decreases. A priori, this two-dimensional eigenspace could split into any two (orthogonal) eigenfunctions from a two-parameter family $\{a_1 u_{13} + a_2 u_{14} : a_1, a_2 \in \mathbb{R}\}$. However, we see from Figs. 7 and 6 that these eigenfunctions appear to split according to the canonical eigenfunctions on the square. This behavior is consistently observed for this homotopy. We will see in Section 3 different behavior for that homotopy.

Additionally, observe the closely bound eigenfunctions in some of our eigenvalue plots. That is, as t varies in our homotopy, we see two eigenfunctions whose eigenvalues remain very close for all t . This effect is puzzling for the authors to explain, and it is unclear whether it only occurs in the lower part of the spectrum. We observe this effect for eigenfunctions 10 and 11 in Fig. 2 and eigenfunctions 5 and 6 in Fig. 5. This effect is not observed in our homotopy of Section 3.

Also note that certain eigenvalues change in similar ways. For instance,

eigenvalues 13,18, and 24 of the circle in the $(1 + +)$ family all have noticeably negative slope around $t = .5$.

This observation indicates that patterns occur in our eigenfunction homotopies. In other words, it seems that sets of similar eigenfunctions behave in similar ways in the homotopies.

In Fig. 7, we depict the homotopy of eigenfunctions of Eigenvalue 13 of the circle in the $(1 + +)$ family. In Fig. 8, we show this same homotopy restricted to the positive x -axis.

In Fig 9, we take the same homotopy as in Figs. 7 and 8, but for simplicity we only examine the nodal set of the eigenfunction. We approximate this nodal set by the inverse image of a small neighborhood of 0 of the form $(-\epsilon, \epsilon)$.

In Fig. 10 we depict the homotopy of Eigenvalue 10 on the circle in the $(1 - -)$ family. In Fig. 11 we show the homotopy of the corresponding nodal set, as in Fig. 9.

Observe from Figs. 1-5 that the endpoints of the graphs of the eigenvalues give a bijection between the eigenfunctions on the circle and those on the square. Since this bijection may encapsulate information about our homotopy or the eigenfunctions themselves, we examine it. For simplicity, we view the correspondences of the nodal sets of the eigenfunctions. Figs. 12-16 displays pictorially some of these correspondences and Table 1 displays all of the data in terms of eigenfunction labels. For instance, we find nontrivial information about the splitting of the two-dimensional eigenspaces on the endpoints (corresponding to $t = 0$ and $t = 1$).

How do we actually determine existence or non-existence of a two-dimensional eigenspace as we vary t in an eigenfunction homotopy? Since different symmetry families do not interact, it is easy to see when two eigenvalues from different symmetry families cross. For instance, if we combine the (non-interacting) eigenvalues of Figs. 1-5 in a single plot, we will definitely have crossings. But for eigenfunctions in the same symmetry family, we cannot rigorously determine from the experimental data whether or not two eigenvalues cross, since we are only approximating the smooth functions F and G in discrete time. Yet, as we vary the discrete time parameter, the graphs of the (lower eigenvalue) eigenfunctions change very slowly. So, if two eigenvalues are far apart, and their corresponding eigenfunctions look similar as we vary t , then (trivially) these two eigenvalues do not attain the same value. For example, in Fig. 1, eigenvalues 1 and 10 on the circle (where $t = 0$) are far apart, and their eigenfunctions look entirely different as we vary t . Therefore, these eigenvalues do not cross.

Subtlety arises when two eigenvalues are very close together. If a multiple eigenvalue exists, our numerical methods will not give us two identical eigenvalues. This effect is a result of the instability of two-dimensional eigenspaces discussed in Section 1. Since we are given approximate solutions to the eigenvalue problem, we will get two distinct eigenvalues which are very close together. Measuring the difference will tell us the approximate (relative) error of our numerical method. Given two nearly identical computed eigenvalues $\tilde{\lambda}_j, \tilde{\lambda}_{j+1}$ at $t = t_0$, we are therefore interested in the quantity

$$E_j = \frac{|\tilde{\lambda}_j - \tilde{\lambda}_{j+1}|}{\tilde{\lambda}_j} \quad (20)$$

For eigenspaces that we know have multiplicity, we find that $E_j \leq 8 \times 10^{-5}$.

Recall from above that, with respect to our eigenvalue data, a collision (see Fig. 19(a)) and a multiplicity are effectively indistinguishable for E_j very small. Therefore, for collisions with E_j around 8×10^{-5} , we are forced to conclude that a multiple eigenvalue occurs. Conversely, if $E_j \gg 8 \times 10^{-5}$, we know that no multiple eigenvalue occurs in a neighborhood of the region we have analyzed.

In Fig. 1, eigenvalues 12 and 13 on the circle (where $t = 0$) become very close around $t = .4$ and $t = .5$. We have observed the discrete homotopy of eigenvalue 12 in Figs. 7, 8 and 9. In all three figures, we see what appears to be a discontinuity in the homotopy around $t = .5$.

This apparent discontinuity occurs since the numerical computations we have used cannot tell the difference between a two-dimensional eigenspace and an almost two dimensional eigenspace. In other words, for two close eigenvalues, the solver combines two distinct eigenfunctions. Our intuition used above can also apply here: quite possibly, an eigenvalue collision is just a perturbation (geometric or otherwise) of a true two-dimensional eigenspace. Once again, this is a manifestation of the superposition effect¹⁰. The data shows two linear combinations of the true eigenfunctions, instead of a separation into two non-interacting eigenspaces. To assuage these concerns, we make higher precision calculations with a higher number of time values t around the potential two-dimensional eigenspace. We then use the relative error of Eq. (20) to determine whether or not a two-dimensional eigenspace occurs. If a two-dimensional eigenspace is determined to occur, we then incorporate the eigenfunction data and the fact that the eigenvalues vary analytically (recall Theorem 3.9,VII.§4.5 of Kato's book⁹). If the higher and lower eigenfunctions swap appearances around the multiple eigenvalue, then the eigenvalues cross. If no such swap occurs, the eigenvalues do not cross. This completes our analysis of the spectral dynamics.

Let us demonstrate the above procedure by example. Along the homotopy H for the $(1 - -)$ family, we see from Fig. 4 that eigenvalues 10 and 11 on the circle ($t = 0$) get very close together at $t = .7$. Our depiction of the homotopy of Eigenvalue 10 on the circle in Fig. 10 again shows ambiguous behavior at $t = .7$. To make our analysis more precise, we solve the eigenvalue problem for H for $t \in \{.6, .62, .64, \dots, .78, .8\}$. In Fig. 17 we show the tenth eigenvalue for these t values, and in Fig. 18 the eleventh eigenvalue. In the time interval $[.6, .8]$, we observe that the tenth and eleventh eigenvalues become very close. For instance, at $t = .72$, the normalized eigenvalues are separated by about $1/10$, giving a relative error $E_{10} \approx .00185 \gg 8 \times 10^{-5}$.

So, we conclude that no two-dimensional eigenspace has occurred within this time interval. For an example with a two-dimensional eigenspace with no apparent crossing (i.e. where the ordering of the two eigenvalues does not change), see Figs 36 and 37 in Section 3.

To summarize the different eigenvalue dynamics, we display Figs. 19 and 20. Fig. 19 shows three different eigenvalue interactions (all from eigenvalue computations), and Fig. 20 shows the gaps between each of the respective pairs of eigenvalues. If we examine the axes of these figures carefully, we see that part (a) has a pair of eigenvalues which do not come close enough together for a two-dimensional eigenspace to occur. This reaffirms our recent observations of Figs. 17 and 18. From these same figures we see that the two eigenfunctions swap identities, so with our intuition from Eq. (3) in mind, we call this interaction a *collision*. In part (b), we know that a two-dimensional eigenspace occurs at $t = .75$, but we see from Figs. 36 and 37 that the eigenfunctions do not swap

identities. Therefore, this is a *non-crossing*. In part (c), we find evidence for a two-dimensional eigenspace, and we observe the swapping of eigenfunction identities in Figs. 32 and 33. Therefore, this is a *crossing*.

We note that the same effect of nearby eigenspaces also occurs on the square. Recall that on the square, we have several two dimensional eigenspaces. So, the choice of two orthogonal eigenfunctions by our numerical method from such an eigenspace amounts to two arbitrary linear combinations of the true eigenfunctions. However, as in Fig. 7, we see that, as we approach the square (around $t = .9$), we approach a particular eigenfunction in a two-dimensional eigenspace on the square. Since the eigenfunctions vary analytically, the homotopy of eigenfunctions therefore selects for us a member of the two dimensional eigenspace on the square. It is then interesting to note that, in our observed data, the eigenfunction thus selected is always a “natural” eigenfunction on the square, i.e. an eigenfunction of the form $\cos \pi ax \cos \pi by \pm \cos \pi bx \cos \pi ay$, rather than a linear combination of two such eigenfunctions. However, in the homotopy of Section 3, we often see that a two-dimensional eigenspace on the square splits into two one-dimensional eigenspaces in the non-“natural” way. More specifically, the numerical evidence shows a few two-dimensional eigenspaces definitely split in a non-canonical way (see Figs. 34 and 35 below). For other examples, the evidence is less striking, but non-canonical splittings still seem to occur in mostly all examples (bold entries in Table 2).

3 SIERPINSKI CARPET HOMOTOPY

Let $A_0 = \{(x, y) \in \mathbb{R}^2 : \max\{|x|, |y|\} \leq \frac{1}{2}\}$ be the unit square centered at the origin. Let $\{f_i\}_{i=1}^8$ denote the usual eight affine linear maps used in the construction of SC , and let

$$A_j = \bigcup_{i=1}^8 f_i A_{j-1}, \quad (21)$$

for $j > 0$, $j \in \mathbb{Z}$. Recall that the Sierpinski carpet SC is defined (as in Section 1) by

$$SC = \bigcap_{i=0}^{\infty} A_i. \quad (22)$$

We would like to deform A_1 continuously into A_0 , and then iterate this procedure for higher A_j . (The choice to make a map $A_1 \rightarrow A_0$ instead of $A_0 \rightarrow A_1$ is for convenience. Also, as stated in Section 1, note that the removal of a single point does not change the Neumann Laplacian.) To construct these deformations, we follow the procedure of Section 2. Let

$$C = \left\{ (x, y) \in \mathbb{R}^2 : x > 0, \frac{\pi}{4} > \tan^{-1}(y/x) > -\frac{\pi}{4} \right\} \cup \{(0, 0)\} \quad (23)$$

so that C is the right “quarter” of the plane. Then let $L = A_1 \cap C$ be the right “quarter” of the picture frame A_1 . Now, define $G(t, x, y) : [0, 1] \times L \rightarrow A_0 \cap C$ by

$$G(t, x, y) = \left(\frac{3}{2}tx - \frac{3}{2}t + 1 \right) \cdot (x, y). \quad (24)$$

Observe that G is a straight line homotopy from the identity map to the map $(x, y) \mapsto ((3/2)x - (1/2)) \cdot (x, y)$. As in Section 2, if we rotate the domain

and range of the map three times by increments of $\pi/2$ radians, we obtain a continuous map $G_0: [0, 1] \times A_1 \rightarrow A_0$. This map is depicted in Fig. 26. To extend G_0 to the remaining A_j , $j > 0$, define $G_j(t, x, y): [0, 1] \times A_{j+1} \rightarrow A_j$ inductively by

$$G_j(t, x, y) = \bigcup_{i=1}^8 f_i \circ G_{j-1}(t, f_i^{-1}(x, y)). \quad (25)$$

In words, we apply G_{j-1} to each of the eight images $\{f_i A_{j-1}\}_{i=1}^8$ used to define A_j . So, for a fixed j , we use $f_i: A_{j-1} \rightarrow A_j$, so that $f_i^{-1}: f_i A_{j-1} \rightarrow A_{j-1}$ is the (well-defined) map in Eq. (25). Finally, since $G_0 = id$ on $\partial A_0 \subset A_1$ for all t , the map G_j is well defined (a priori, each $G_j(t, \cdot, \cdot)$ has two definitions for certain $(x, y) \in B_j$). The maps G_1 through G_3 are depicted in Figs. 27 through 29 respectively.

As in Section 2 we see that, for each j , the eigenvalues and eigenvectors of G_j can be represented as functions holomorphic in t . However, since the domains of G_j and G_{j+1} only meet continuously, the eigenvalues only vary continuously around $\text{im}(G_j(1, \cdot, \cdot)) = \text{im}(G_{j+1}(0, \cdot, \cdot))$. We further note that $G_j(1, x, y)$ maps B_j to A_{j+1} as expected. Finally, to stay consistent with Section 2, we refer to $G_j(t, x, y)$ below as $G_j(1-t, x, y)$ as defined in the previous few paragraphs (we have already used this convention in the caption of Figs. 19 and 20).

As above, our domains $\{B_j\}_{j=0}^\infty$ are invariant under the D_4 symmetry group. In our computations, we restrict each B_j to the sector $0 \leq \theta \leq \pi/4$ in polar coordinates, for the 1-dimensional representations. We impose our four combinations of boundary conditions on the intersection of our domain with the rays $\theta = 0$ and $\theta = \pi/4$. For the 2-dimensional representation, our fundamental domain is $B_j \cap L$. We impose Neumann boundary conditions on the ray $\theta = \pi/4$ and Dirichlet conditions on the ray $\theta = -\pi/4$.

For all fundamental domains, we place Neumann boundary conditions on all remaining edges. Notice that once again, our fundamental domains are simply connected for $j = 0$. Therefore, as in Theorem 6.4 of the reference⁴, we should expect no eigenvalue crossings along this homotopy (for each individual symmetry family). Since eigenvalue crossings do in fact occur, this suggests that there is something exceptional (i.e. non-generic) about our domains. The appearance of these crossings could be related to the quantum-classical correspondence principle. More specifically, since the billiard flow is not ergodic in phase space, this may suggest a dense number of crossings.

In Figs. 21 to 25 we display the observed crossing of eigenvalues for the five symmetry families $(1+, +, 1+, -, 1-, +, 1-, -, 2)$ with eigenvalues divided by π^2 . We collect the data of $G_j(t, \cdot, \cdot)$ for $j = 0, 1, 2, 3$ and for $t \in \{k/10\}_{k=0}^{10}$. Observe that, in the bottom of the spectrum, the incidence of crossings decreases as j increases. More specifically, the incidence of non-crossings grows exponentially. Also observe that, indeed, the eigenvalues of G_j and G_{j+1} meet in a continuous but non-differentiable manner.

In Figs. 26-29, we show the homotopy of eigenfunctions of Eigenvalue 4 in the $(1+, +)$ family for G_0 through G_3 . This eigenfunction exhibits the typical, expected behavior. The function changes a great deal for G_j with j small, and then as j grows large the eigenfunction maintains the same appearance. However, the eigenvalue continues changing, as expected.

In Fig. 30 we show the nodal homotopy corresponding to Fig. 26. With a low eigenvalue, this eigenfunction exhibits minimal irregularity during the

homotopy. In Fig. 31 we show the homotopy of 26 restricted to the line $\{(x, y) \in \mathbb{R}^2: 0 \leq x \leq 1/2\}$.

It is interesting to note how the two dimensional eigenspaces split for $G_0(t, \cdot, \cdot)$ as we move t from 0 to some small $\epsilon > 0$. In Section 2, we saw a “canonical splitting” for the given homotopy. However, the eigenfunctions for $G_0(\epsilon, \cdot, \cdot)$ for two dimensional eigenspaces do not resemble the natural eigenfunctions of $G_0(0, \cdot, \cdot)$. For example, in Figs. 32 and 33, we see the two-dimensional eigenspace on the square split with an apparent discontinuity. In Figs. 34 and 35, we see a (non-canonical) splitting of the two-dimensional eigenspace on the square. If this were a canonical splitting, we would have the $(10, 0)$ and $(8, 6)$ eigenfunctions. However, there is no direct resemblance of our computed eigenfunctions and the canonical ones. In fact, around $t = .1$, these eigenfunctions cross again, since the relative error between the eigenvalues is about $6.4 \times 10^{-5} < 8 \times 10^{-5}$ (recall the discussion around Eq. (20)). Finally, in Figs. 36 and 37 we show the homotopy around an (analytically determined) two-dimensional eigenspace at $t = .75$. It is not hard to find infinite sets of such eigenspaces for any rational $t \in (0, 1)$.

4 CONCLUSIONS

We now summarize our results. In both of our homotopies, we preserve the D_4 symmetry of the domains. This allows us to split the eigenfunctions on these domains into five non-interacting families. That is, the behavior of eigenfunctions in one symmetry family along the homotopy does not affect the other families. The following is then clear: eigenvalues of one symmetry family definitely cross with eigenvalues of other symmetry families. However, the numerical evidence leads us to speculate on the individual symmetry families as follows. When we deform the circle to the square, we observe no intermediate two-dimensional eigenspaces. However, when we deform the square to the picture frame (a square with a smaller square removed from the center) we do find intermediate two-dimensional eigenspaces. In fact, analytically one can easily find an arbitrarily large number nontrivial multiplicity eigenspaces for a fixed rational time.

When we observe our domains, we see that the deformation of the circle to the square is a convex diamond-shaped region for all $t \in [0, 1]$. In fact, for $t \in (0, 1)$, the region is a diamond with four edges, each of which is a half-ellipse. However, as we map the square A_0 to the picture frame A_1 via H , we always have a rational polygon (a polygon with angles which are rational multiples of π). Mapping A_i to A_{i+1} via G_i always yields a rational domain with a finite number of flat edges (which is now multiply connected for $i \geq 1$). Recall: (a) after reducing multiplicities due to symmetry, we observe eigenvalues of nontrivial multiplicity for G_0 but not H . Also, (b) for G_i we observe non-canonical splitting of two-dimensional eigenspaces of the square, and for H we only observe canonical splitting.

With respect to observation (a), it is tempting to make a connection between the appearance of eigenvalue multiplicity and ergodicity of the billiard flow, but such a connection is unclear. Such considerations seem related to the quantum-classical correspondence, and some conjectures discussed in the reference¹¹. In particular, the author mentions that, for the bottom part of the spectrum, the eigenvalues for integrable billiards may follow a Poisson distribution, while the eigenvalues for a chaotic system may follow a GOE (Gaussian Orthogonal

Ensemble) distribution. With respect to observation (b), the authors have no clear explanation.

We have just discussed possible connections between ergodicity of billiard flow and eigenvalue properties. Such connections are collected under the so-called quantum-classical correspondence. Perhaps extending these connections further, we discuss the localization and near-localization (or scarring) of eigenfunctions. For the standard Laplacian on the Sierpinski Gasket (SG), many eigenfunctions are localized¹². Indeed, it appears that for many symmetric PCF fractals, the symmetry of the fractal and the capability to break it into disjoint pieces by removing finitely many points contributes to the localization of eigenfunctions. In contrast, we have SC , which is a symmetric non-PCF fractal (intuitively, this means it cannot be broken up into smaller pieces by removing finitely many points).

We now ask: do the “stronger” connectivity properties of SC forbid localized eigenfunctions? We believe the numerical evidence from this paper suggests, yes. Indeed, no localized eigenfunctions appear in the computations. If the outer approximation method of⁵ actually works, then this observation finds strong support. For possible counter-evidence, let us consider the results of¹³, which imply that any rectangular portion of a domain almost always exhibits eigenfunction scarring (that is, having mass concentrated in the domain in a non-equidistributed way). This would imply that the number of scarred modes for our domains should increase exponentially as $j \rightarrow \infty$ as in Eq. (17). However, it is unclear whether a scarred eigenfunction for a fixed j would remain scarred as j increases. If the outer approximation method of⁵ holds, then the eigenfunction scarring may have repercussions for the eigenfunctions on SC , even though strict localization may not occur.

Although it may seem unfortunate that we are not able to arrive at any coherent description, even just conjectural, relating the behavior of eigenfunctions joined by a homotopy, there is also a more optimistic conclusion: the connection is rather complicated, and requires further investigation. We hope that the data we present will inspire further investigation. (Data available in full at www.math.cornell.edu/~smh82)

References

- [1] T. Tao, *Research Weblog* <<http://terrytao.wordpress.com/>>
- [2] Y. Colin de Verdière, *Sur une hypothèse de transversalité d’Arnol’d*. (French) [On a transversality conjecture of Arnol’d] *Comment. Math. Helv.* **63** (1988), no. 2, 184-193. MR MR0948776
- [3] P. D. Lamberti and M. Lanza De Cristoforis *Persistence of eigenvalues and multiplicity in the Dirichlet problem for the Laplace operator on nonsmooth domains*. (English summary) *Math. Phys. Anal. Geom.* **9** (2006), no. 1, 65-94. MR MR2245262
- [4] M. Teytel, *How rare are multiple eigenvalues?* *Comm. Pure Appl. Math.* **52** (1999), no. 8, 917-934. MR MR1686977
- [5] T. Berry, S. Heilman, and R. S. Strichartz, *Outer Approximation of the Spectrum of a Fractal Laplacian*, (to appear) *Exp. Math.*

- [6] M.T. Barlow and R.F. Bass, *The construction of Brownian motion on the Sierpinski carpet*, Ann. de l'Institut H. Poincaré **25** (1989), 225-257. MR MR1023950 (91d:60183)
- [7] M. T. Barlow, R. F. Bass, T. Kumagai, and A. Teplyaev, *Uniqueness of Brownian motion on Sierpinski carpets* (preprint)
- [8] R. F. Bass, *Diffusions on the Sierpinski carpet*. (English summary) Trends in probability and related analysis (Taipei, 1996), 1-34, World Sci. Publ., River Edge, NJ, 1997. MR MR1616273
- [9] T. Kato, *Perturbation Theory for Linear Operators*, (Springer-Verlag, 1966). MR MR0203473
- [10] A. Bäcker, R. Schubert, and P. Stifter, *On the number of bouncing ball modes in billiards*, J. Phys. A **30** (1997), no. 19, 6783-6795. MR MR1481345
- [11] P. Sarnak, *Arithmetic quantum chaos*. (English summary) The Schur lectures (1992) (Tel Aviv), 183-236, Israel Math. Conf. Proc., **8**, Bar-Ilan Univ., Ramat Gan, 1995. MR MR1321639
- [12] R. S. Strichartz, *Differential Equations on Fractals: A Tutorial*, Princeton University Press, Princeton, NJ 2006. MR MR2246975 (2007f:35003)
- [13] A. Hassell and Luc Hilgairt, *Ergodic billiards that are not quantum unique ergodic*, (preprint)

Eigenvalue Correspondences										
Eigenvalue Number on Circle	(1 + +) Family		(1 - -) Family		(1 - +) Family		(1 + -) Family		(2) Family	
	Circle	Square	Circle	Square	Circle	Square	Circle	Square	Circle	Square
1	(1, 0)	(2, 0)	(0, 4)	(3, 1)	(0, 2)	(1, 1)	(0, 2)	(2, 0)	(0, 1)	(1, 0)
2	(0, 4)	(2, 2)	(1, 4)	(5, 1)	(1, 2)	(3, 1)	(1, 2)	(4, 0)	(0, 3)	(2, 1)
3	(2, 0)	(4, 0)	(0, 8)	(5, 3)	(0, 6)	(3, 3)	(0, 6)	(4, 2)	(1, 1)	(3, 0)
4	(1, 4)	(4, 2)	(2, 4)	(7, 1)	(2, 2)	(5, 1)	(2, 2)	(6, 0)	(0, 5)	(3, 2)
5	(0, 8)	(4, 4)	(0, 12)	(7, 3)	(1, 6)	(5, 3)	(1, 6)	(6, 2)	(1, 3)	(4, 1)
6	(3, 0)	(6, 0)	(1, 8)	(7, 5)	(0, 10)	(5, 5)	(0, 10)	(6, 4)	(2, 1)	(4, 3)
7	(2, 4)	(6, 2)	(3, 4)	(9, 1)	(3, 2)	(7, 1)	(3, 2)	(8, 0)	(0, 7)	(5, 0)
8	(4, 0)	(6, 4)	(2, 8)	(9, 3)	(2, 6)	(7, 3)	(2, 6)	(8, 2)	(1, 5)	(5, 2)
9	(0, 12)	(8, 0)	(0, 16)	(9, 5)	(0, 14)	(7, 5)	(0, 14)	(8, 4)	(0, 9)	(6, 1)
10	(1, 8)	(8, 2)	(1, 12)	(11, 1)	(4, 2)	(9, 1)	(4, 2)	(8, 6)	(2, 3)	(5, 4)
11	(3, 4)	(6, 6)	(4, 4)	(9, 7)	(1, 10)	(9, 3)	(1, 10)	(10, 0)	(3, 1)	(6, 3)
12	(5, 0)	(8, 4)	(3, 8)	(11, 3)	(3, 6)	(7, 7)	(3, 6)	(10, 2)	(0, 11)	(7, 0)
13	(2, 8)	(10, 0)	(0, 20)	(11, 5)	(5, 2)	(9, 5)	(5, 2)	(10, 4)	(1, 7)	(7, 2)
14	(0, 16)	(8, 6)	(5, 4)	(13, 1)	(0, 18)	(11, 1)	(0, 18)	(10, 6)	(2, 5)	(6, 5)
15	(1, 12)	(10, 2)	(2, 12)	(11, 7)	(2, 10)	(11, 3)	(2, 10)	(12, 0)	(3, 3)	(7, 4)
16	(4, 4)	(10, 4)	(1, 16)	(13, 3)	(1, 14)	(9, 7)	(1, 14)	(12, 2)	(4, 1)	(8, 1)
17	(6, 0)	(8, 8)	(4, 8)	(13, 5)	(4, 6)	(11, 5)	(4, 6)	(12, 4)	(0, 13)	(8, 3)
18	(3, 8)	(10, 6)	(6, 4)	(11, 9)	(6, 2)	(9, 9)	(6, 2)	(10, 8)	(1, 9)	(9, 0)
19	(0, 20)	(12, 0)	(3, 12)	(13, 7)	(3, 10)	(13, 1)	(3, 10)	(12, 6)	(2, 7)	(9, 2)
20	(5, 4)	(12, 2)	(0, 24)	(15, 1)	(0, 22)	(11, 7)	(0, 22)	(14, 0)	(0, 15)	(7, 6)
21	(2, 12)	(12, 4)			(2, 14)	(13, 3)	(2, 14)	(14, 2)	(3, 5)	(8, 5)
22	(7, 0)	(10, 8)			(5, 6)	(13, 5)	(5, 6)	(12, 8)	(1, 11)	(9, 4)
23	(1, 16)	(12, 6)								
24	(4, 8)	(14, 0)								
25	(6, 4)									

Table 1: Table of Eigenfunction Correspondences: For the Circle, $(a, b) \leftrightarrow J_b(\lambda_{n,ar}) \cos(2\pi b\theta)$. For the Square, $(a, b) \leftrightarrow \cos(\pi ax) \cos(\pi by) \pm \cos(\pi ay) \cos(\pi bx)$, (+ in columns 1, 3, - in columns 2, 4). Two dimensional eigenspaces in bold.

Eigenvalue Correspondences																														
(1 + +) Family					(1 - -) Family					(1 + -) Family					(1 - +) Family					(2) Family										
Eigfcn on Square	A_0	A_1	A_2	A_3	A_4	Eigfcn on Square	A_0	A_1	A_2	A_3	A_4	Eigfcn on Square	A_0	A_1	A_2	A_3	A_4	Eigfcn on Square	A_0	A_1	A_2	A_3	A_4	Eigfcn on Square	A_0	A_1	A_2	A_3	A_4	
(2, 0)	1	1	1	1	1	(3, 1)	1	1	1	1	1	(2, 0)	1	1	1	1	1	(1, 1)	1	1	1	1	1	(1, 0)	1	1	1	1	1	
(2, 2)	2	2	2	2	2	(5, 1)	2	2	2	2	2	(4, 0)	2	2	2	2	2	(3, 1)	2	2	2	2	2	(2, 1)	2	2	2	2	2	
(4, 0)	3	3	3	3	3	(5, 3)	3	3	3	3	3	(4, 2)	3	3	3	3	3	(3, 3)	3	3	3	3	3	(3, 0)	3	3	3	3	3	
(4, 2)	4	4	4	4	4	(7, 1)	4	4	4	4	4	(6, 0)	4	4	4	4	4	(5, 1)	4	4	4	4	4	(3, 2)	4	4	4	4	4	
(4, 4)	5	5	6	6	6	(7, 3)	5	5	5	5	5	(6, 2)	5	5	5	5	5	(5, 3)	5	5	5	5	5	(4, 1)	5	5	5	5	5	
(6, 0)	6	6	5	5	5	(7, 5)	6	6	6	6	6	(6, 4)	6	6	6	6	6	(7, 1)	6	6	6	6	6	(4, 3)	6	7	7	7	7	
(6, 2)	7	7	7	7	7	(9, 1)	7	7	7	7	7	(8, 0)	7	7	7	7	7	(5, 5)	7	7	7	7	7	(5, 0)	7	6	6	6	6	
(6, 4)	8	8	8	8	8	(9, 3)	8	8	8	8	8	(8, 2)	8	8	8	8	8	(7, 3)	8	8	8	8	8	(5, 2)	8	8	8	8	8	
(8, 0)	9	9	11	11	11	(9, 5)	9	9	9	9	9	(8, 4)	9	9	9	9	9	(7, 5)	9	9	9	9	9	(6, 1)	9	9	9	9	9	
(8, 2)	10	10	9	9	9	(11, 1)	10	10	10	10	10	(10, 0)	10	10	10	10	10	(9, 1)	10	10	10	10	10	(5, 4)	10	10	11	11	11	
(6, 6)	11	11	10	10	10	(9, 7)	11	11	11	11	11	(8, 6)	11	11	11	11	11	(9, 3)	11	11	11	11	11	(6, 3)	11	11	10	10	10	
(8, 4)	13	13	13	13	13	(11, 3)	12	12	12	12	12	(10, 2)	12	12	12	13	13	(7, 7)	12	12	12	12	12	(7, 0)	12	12	12	12	12	
(?, ?)	13	14	14	14	14	(11, 5)	13	13	13	13	13	(10, 4)	13	13	14	14	14	(9, 5)	13	13	13	13	13	(7, 2)	13	13	13	13	13	
(?, ?)	14	13	13	13	13	(13, 1)	14	15	15	15	15	(10, 6)	14	14	13	12	12	(11, 1)	14	14	14	14	14	(6, 5)	14	14	14	14	14	
(10, 2)	15	15	15	15	15	(11, 7)	15	14	14	14	14	(12, 0)	15	15	15	15	15	(11, 3)	15	15	15	15	15	(7, 4)	15	15	15	15	15	
(10, 4)	16	16	18	19	19	(13, 3)	16	16	16	16	16	(12, 2)	16	16	16	16	16	(9, 7)	16	16	16	16	16	(8, 1)	16	16	16	16	16	
(8, 8)	17	17	16	16	16	(13, 5)	17	17	17	17	17	(12, 4)	17	17	18	18	18	(11, 5)	17	17	17	17	17	(8, 3)	17	17	17	17	17	
(10, 6)	18	18	17	17	17	(11, 9)	18	18	18	19	19	(10, 8)	18	18	17	17	17	(9, 9)	18	18	18	18	18	(9, 0)	18	18	18	18	18	
(12, 0)	19	19	19	18	18	(13, 7)	19	19	20	20	20	(12, 6)	19	19	19	19	19	(11, 7)	19	20	20	20	20	(7, 6)	19	19	19	19	19	
(12, 2)	20	20	26	26	26	(15, 1)	20	20	19	18	18	(14, 0)	20	20	20	20	20	(13, 1)	20	19	19	19	19	(9, 2)	20	21	21	21	21	
(12, 4)	21	21	20	20	20	(15, 3)	21	21	21	21	21	(14, 2)	21	21	21	21	21	(13, 3)	21	21	21	21	21	(8, 5)	21	20	20	20	20	
(10, 8)	22	22	21	21	21	(13, 9)	22	22	22	22	22	(12, 8)	22	22	22	22	22	(13, 5)	22	22	22	22	22	(9, 4)	22	22	22	22	22	
(12, 6)	23	23	22	22	22	(15, 5)	23	23	23	23	23	(14, 4)	23	23	23	23	23	(11, 9)	23	23	24	23	23	(10, 1)	23	23	23	23	23	
(14, 0)	24	24	23	23	23	(15, 7)	24	24	26	26	26	(14, 6)	24	24	24	24	24	(13, 7)	24	24	23	26	26	(10, 3)	24	24	26	26	26	
						(17, 1)	25	25	25	25	25	(12, 10)	25	25	25	25	25	(15, 1)	25	25	25	24	24	(8, 7)	25	25	24	24	24	
						(13, 11)	26	26	27	27	27							(15, 3)	26	26	26	25	25							
						(17, 3)	27	27	24	24	24							(11, 11)	27	27	27	27	27							
						(15, 9)	28	28	28									(

Table 2: Table of Eigenfunction Correspondences: For the Square, $(a, b) \leftrightarrow \cos(\pi ax) \cos(\pi by) \pm \cos(\pi ay) \cos(\pi bx)$, (+ in columns 1, 4, - in columns 2, 3). Two-dimensional eigenspaces in bold. Question marks denote blatantly non-canonical splitting of a two-dimensional eigenspace

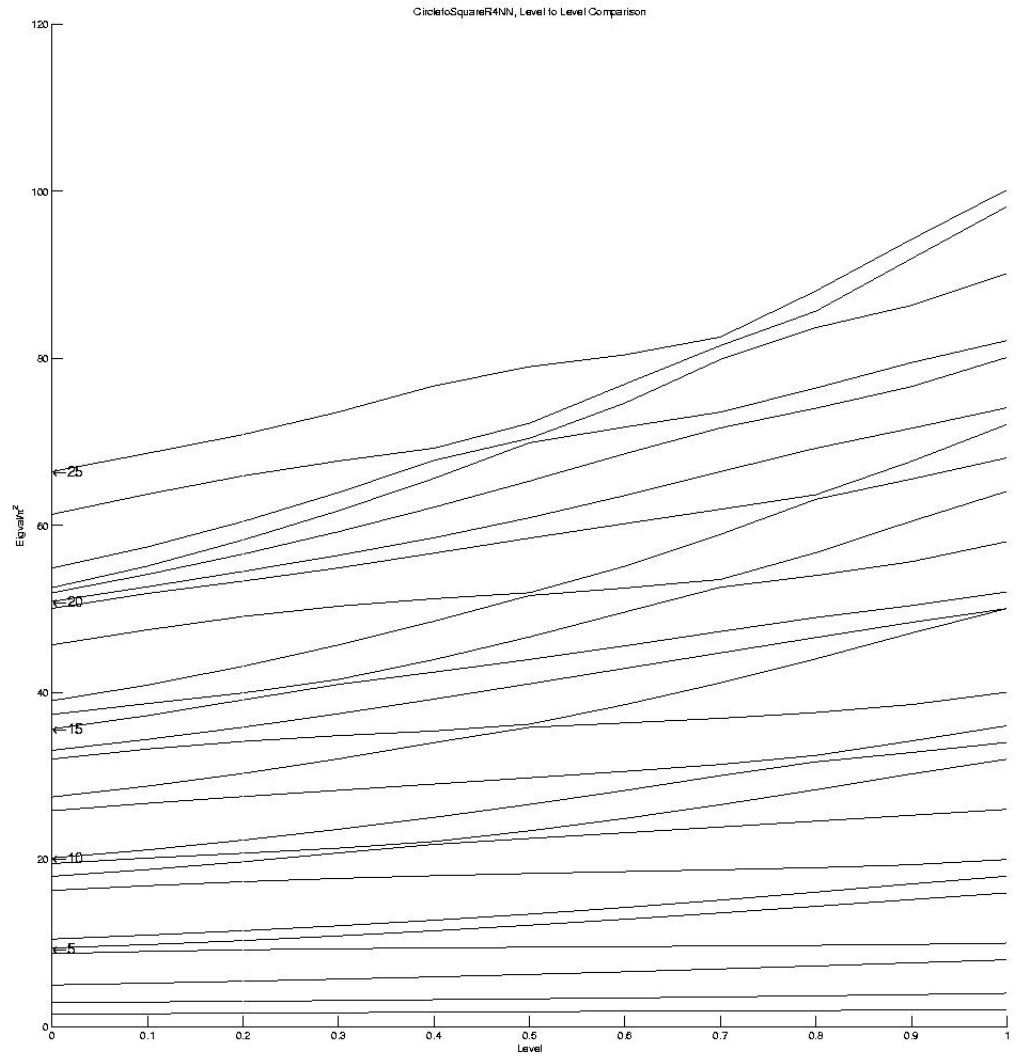


Figure 1: (1 + +) Eigenvalue Summary Plot. Circle ($t = 0$), Square ($t = 1$)

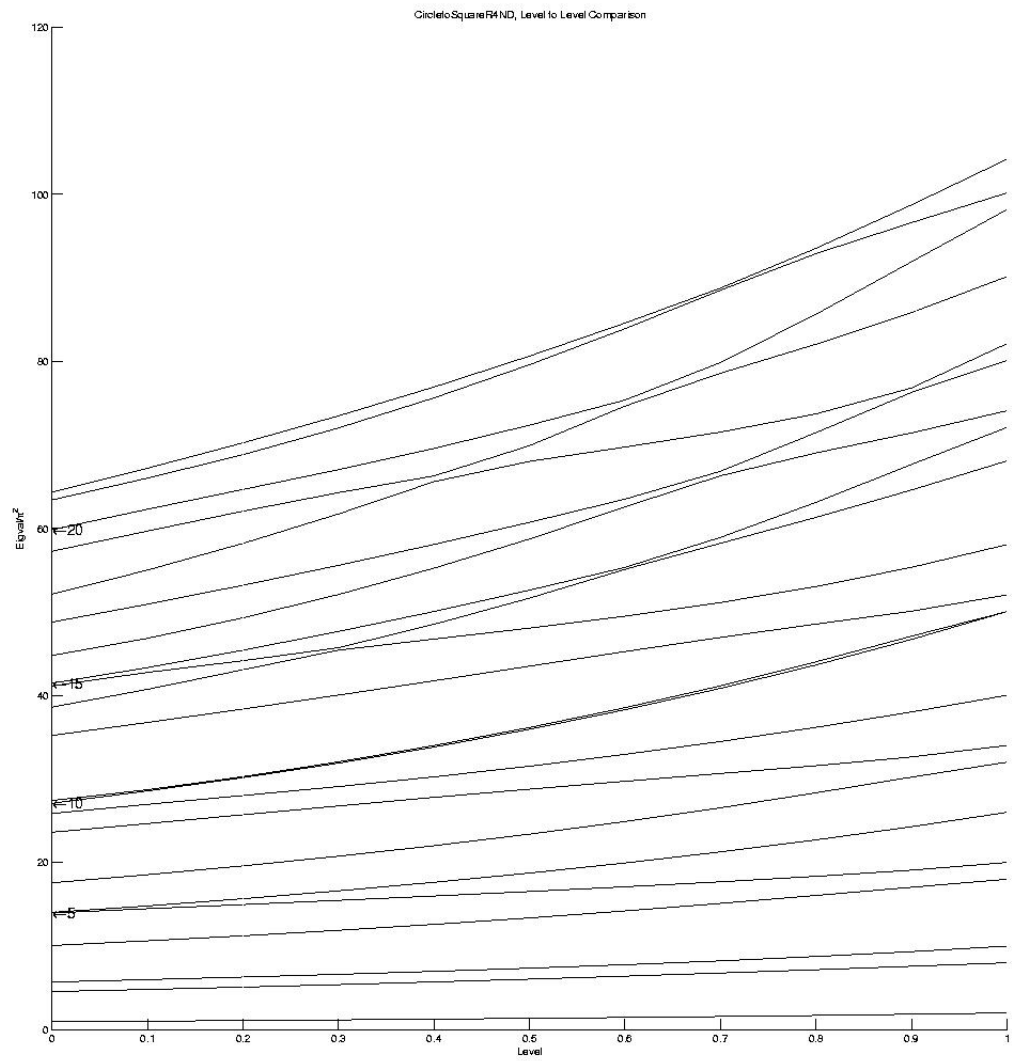


Figure 2: $(1 + -)$ Eigenvalue Summary Plot

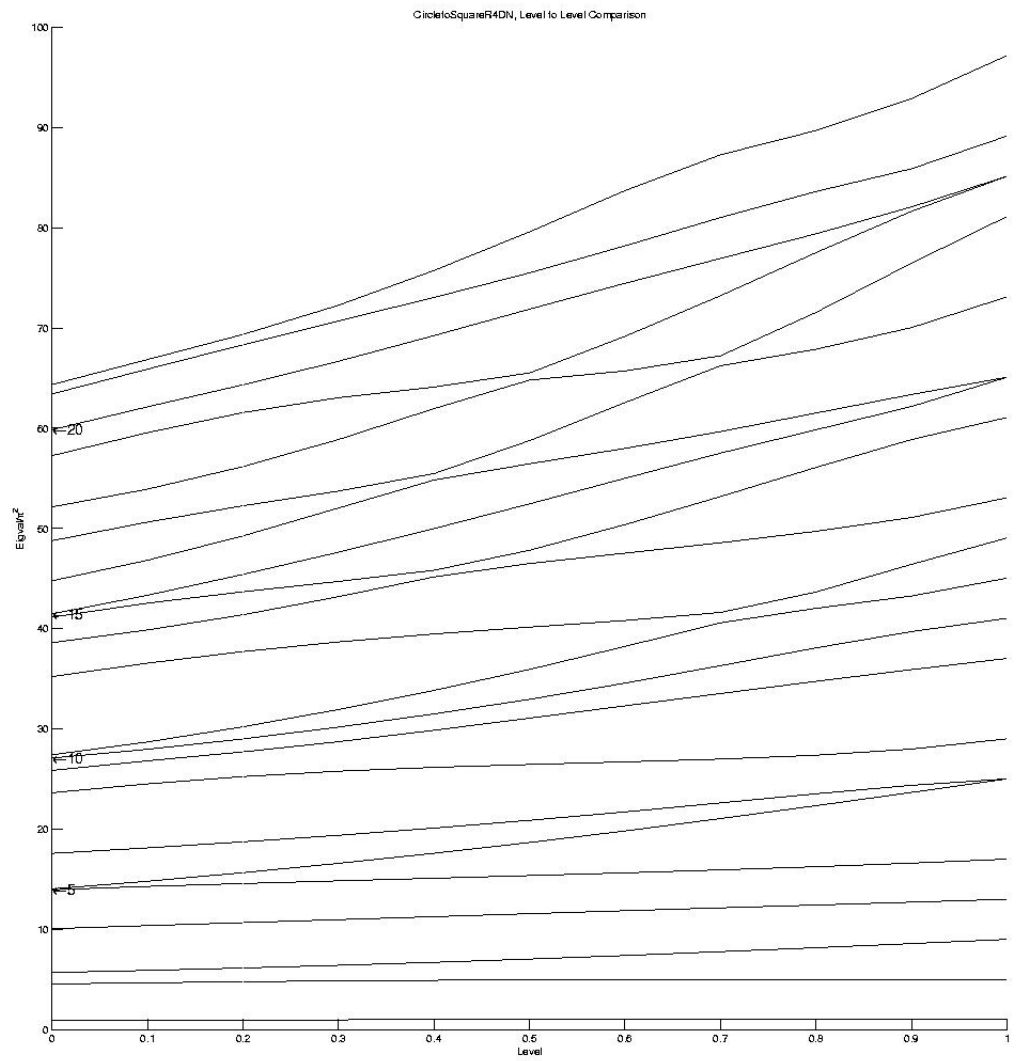


Figure 3: (1 - +) Eigenvalue Summary Plot

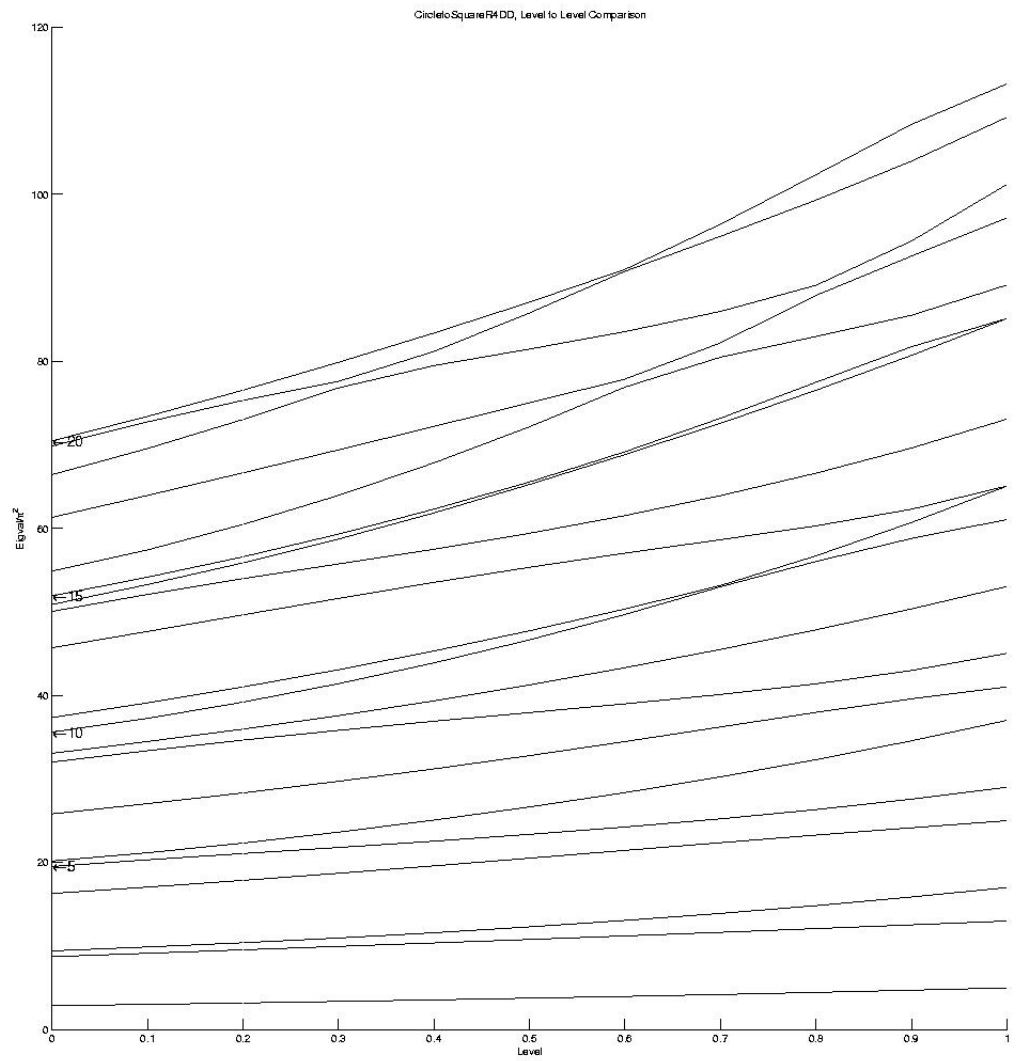


Figure 4: (1 - -) Eigenvalue Summary Plot

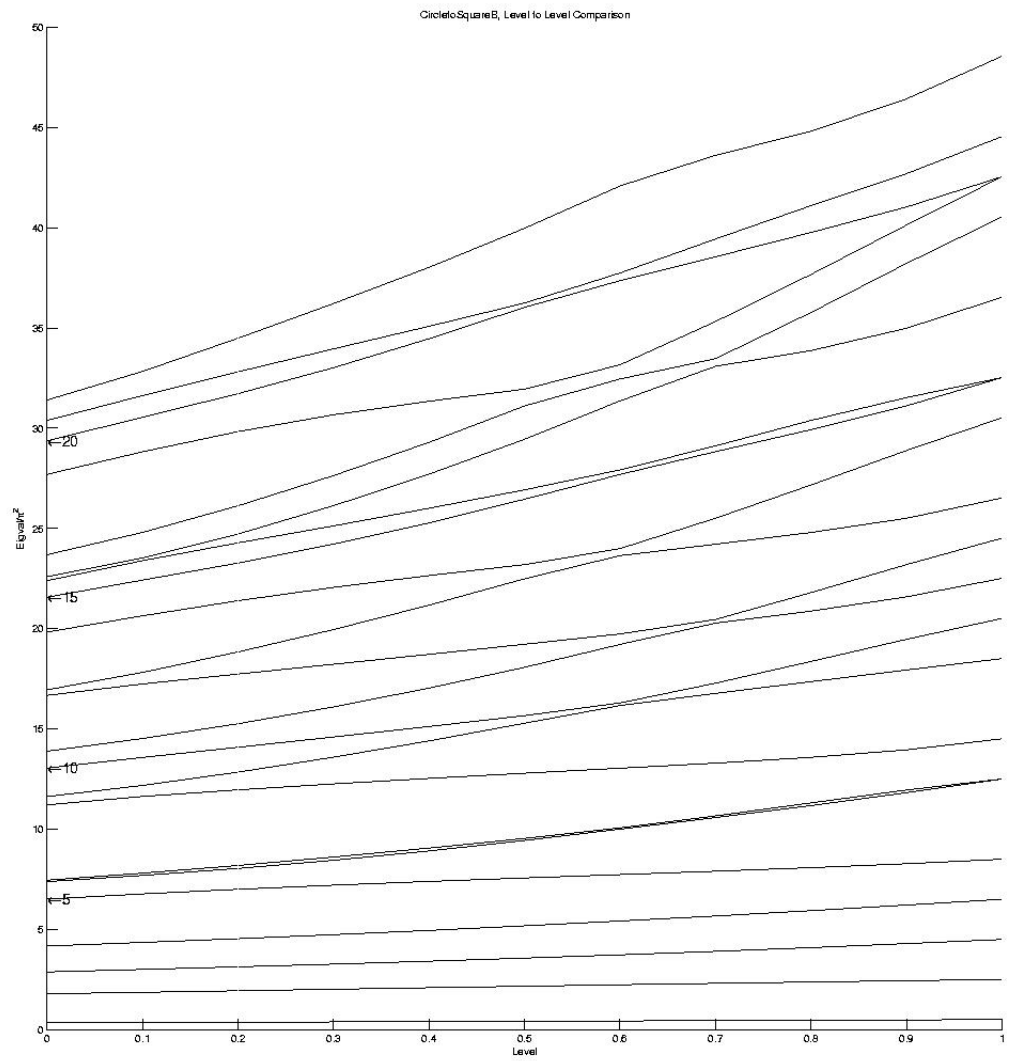


Figure 5: (2) Eigenvalue Summary Plot

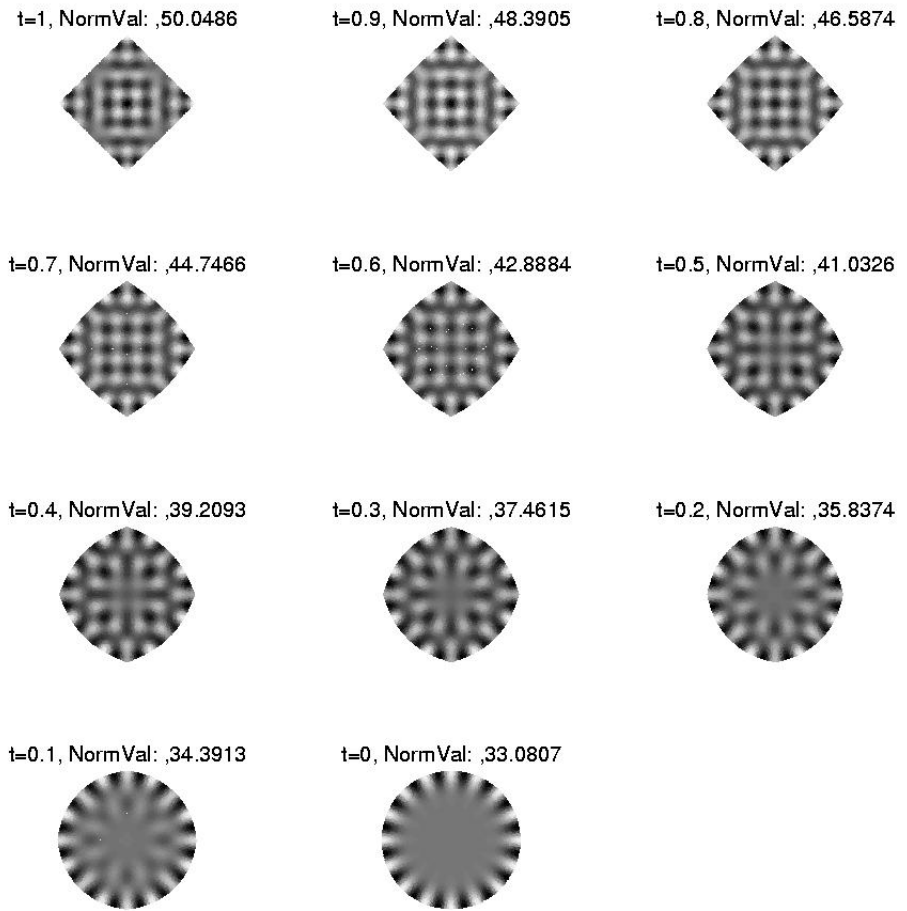
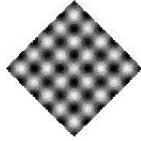
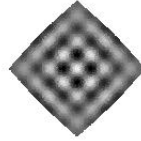


Figure 6: $(1 + +)$ EigVal 14 Homotopy

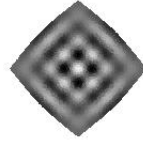
t=1, NormVal: ,50.0434



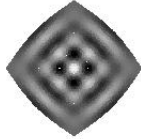
t=0.9, NormVal: ,47.1085



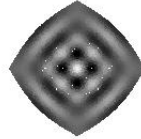
t=0.8, NormVal: ,44.0334



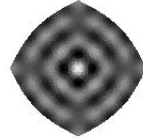
t=0.7, NormVal: ,41.1562



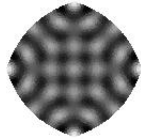
t=0.6, NormVal: ,38.5407



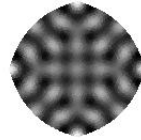
t=0.5, NormVal: ,36.2063



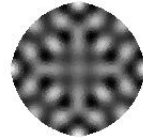
t=0.4, NormVal: ,35.3945



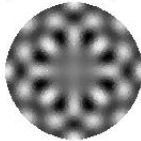
t=0.3, NormVal: ,34.8359



t=0.2, NormVal: ,34.1508



t=0.1, NormVal: ,33.2285



t=0, NormVal: ,32.0286

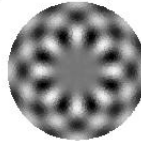


Figure 7: $(1 + +)$ EigVal 13 Homotopy

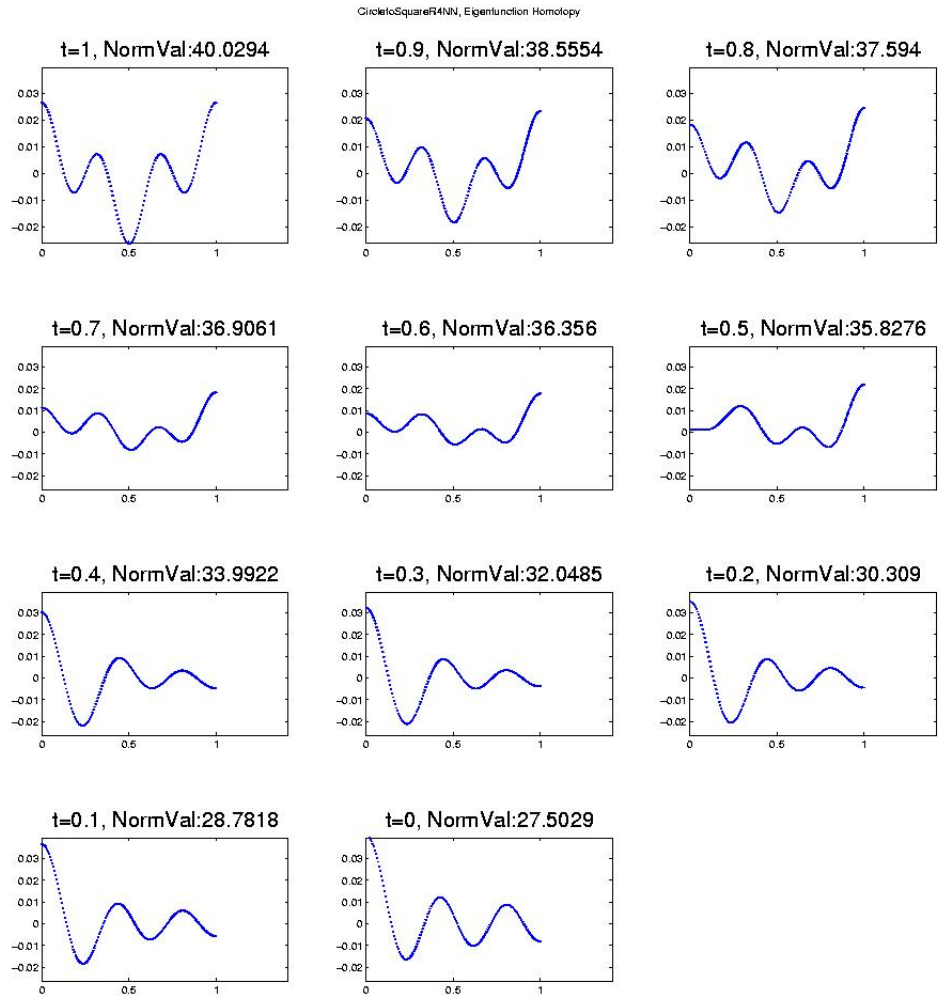
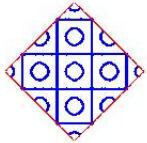
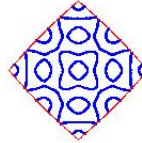


Figure 8: $(1 + +)$ EigVal 13 Homotopy, Restricted to a Line

t=1, NormVal: ,40.0294



t=0.9, NormVal: ,38.5554



t=0.8, NormVal: ,37.594



t=0.7, NormVal: ,36.9061



t=0.6, NormVal: ,36.356



t=0.5, NormVal: ,35.8276



t=0.4, NormVal: ,33.9922



t=0.3, NormVal: ,32.0485



t=0.2, NormVal: ,30.309



t=0.1, NormVal: ,28.7818



t=0, NormVal: ,27.5029

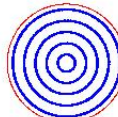
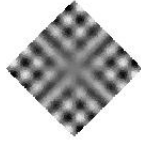
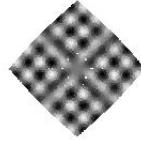


Figure 9: (1 + +) EigVal 13 Nodal Homotopy

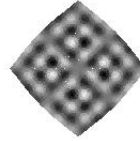
t=1, NormVal: ,61.0655



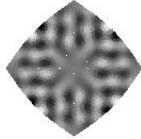
t=0.9, NormVal: ,58.7969



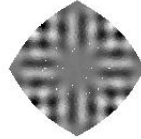
t=0.8, NormVal: ,56.0372



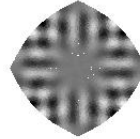
t=0.7, NormVal: ,53.0124



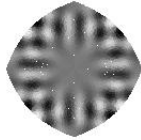
t=0.6, NormVal: ,49.6933



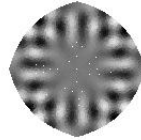
t=0.5, NormVal: ,46.6576



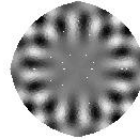
t=0.4, NormVal: ,43.9053



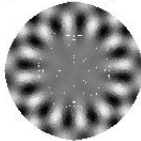
t=0.3, NormVal: ,41.4205



t=0.2, NormVal: ,39.2064



t=0.1, NormVal: ,37.2674



t=0, NormVal: ,35.6248

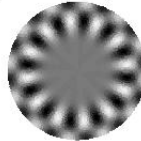
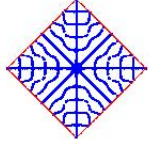
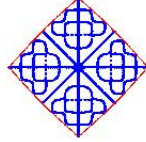


Figure 10: (1 - -) EigVal 10 Homotopy

t=1, NormVal: ,61.0655



t=0.9, NormVal: ,58.7969



t=0.8, NormVal: ,56.0372



t=0.7, NormVal: ,53.0124



t=0.6, NormVal: ,49.6933



t=0.5, NormVal: ,46.6576



t=0.4, NormVal: ,43.9053



t=0.3, NormVal: ,41.4205



t=0.2, NormVal: ,39.2064



t=0.1, NormVal: ,37.2674



t=0, NormVal: ,35.6248



Figure 11: (1 -) EigVal 10 Nodal Homotopy

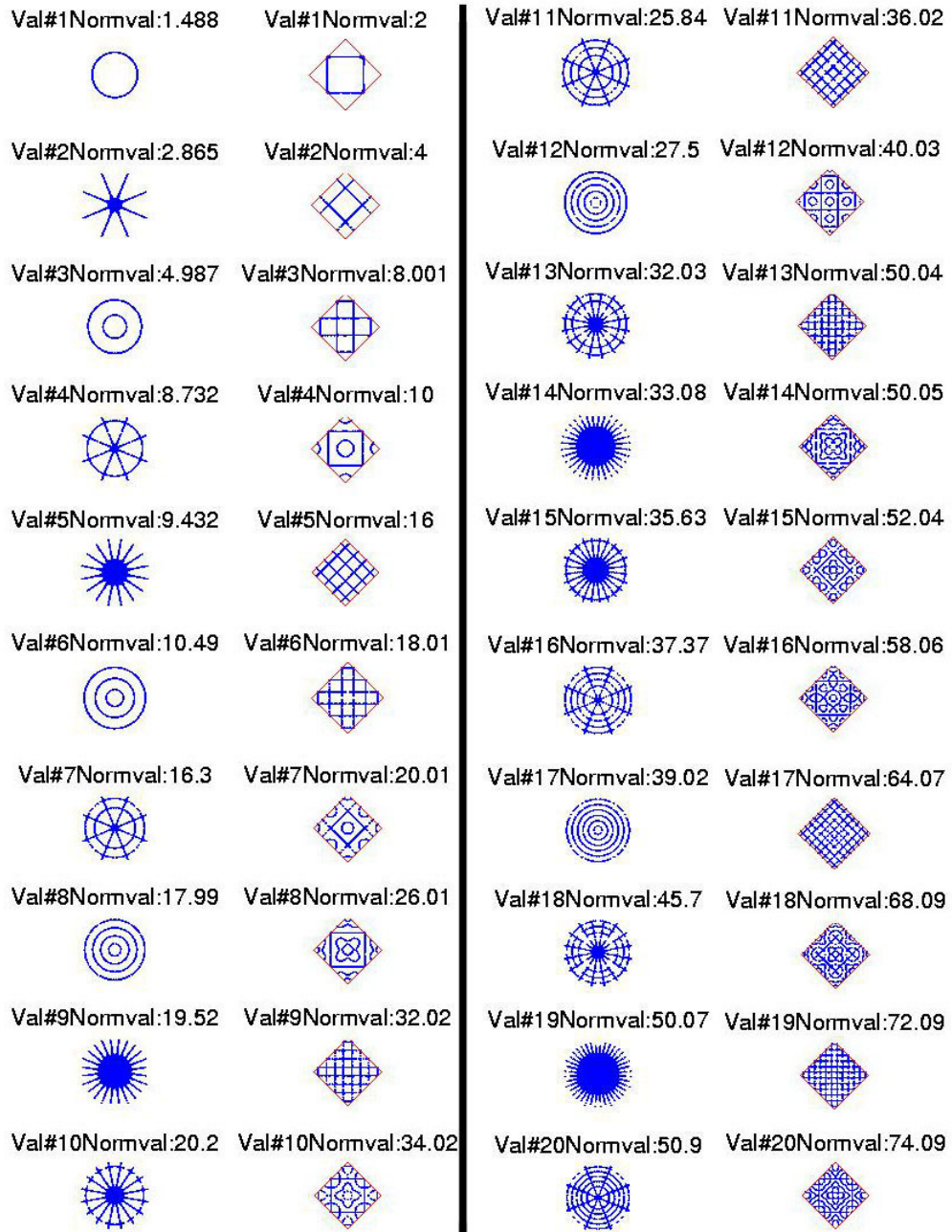


Figure 12: $(1 + +)$ Eigenfunction correspondences

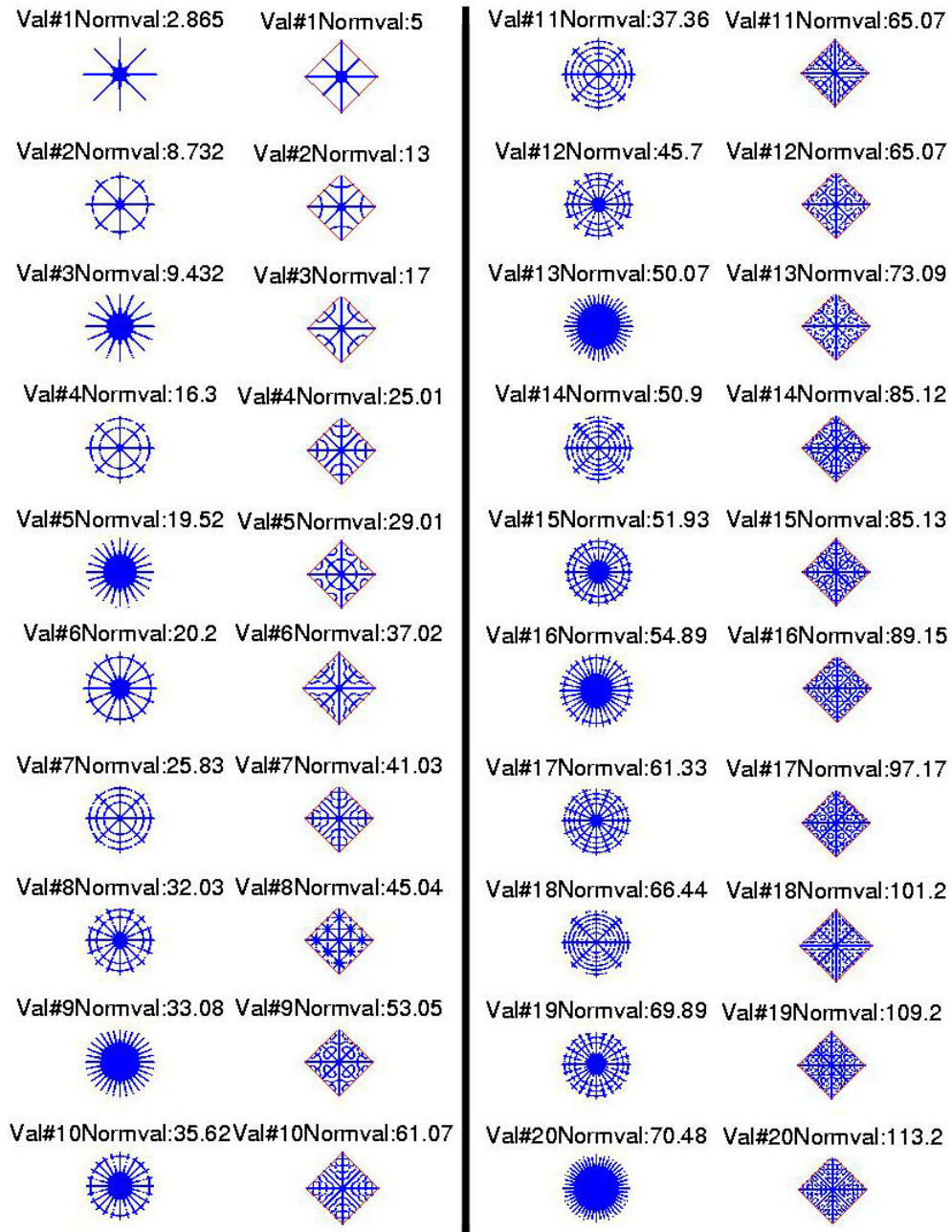


Figure 13: (1 - -) Eigenfunction correspondences

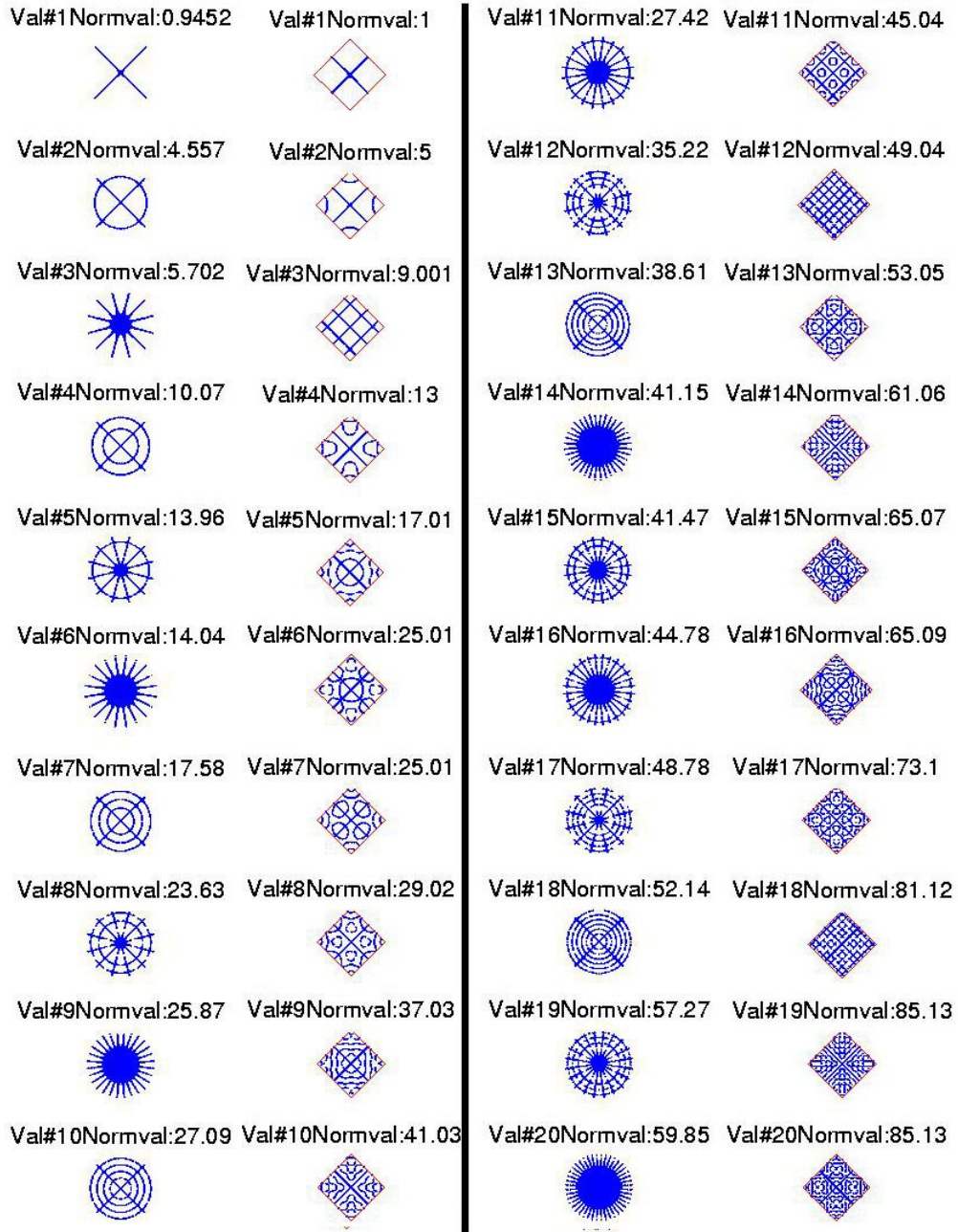


Figure 14: $(1 - +)$ Eigenfunction correspondences

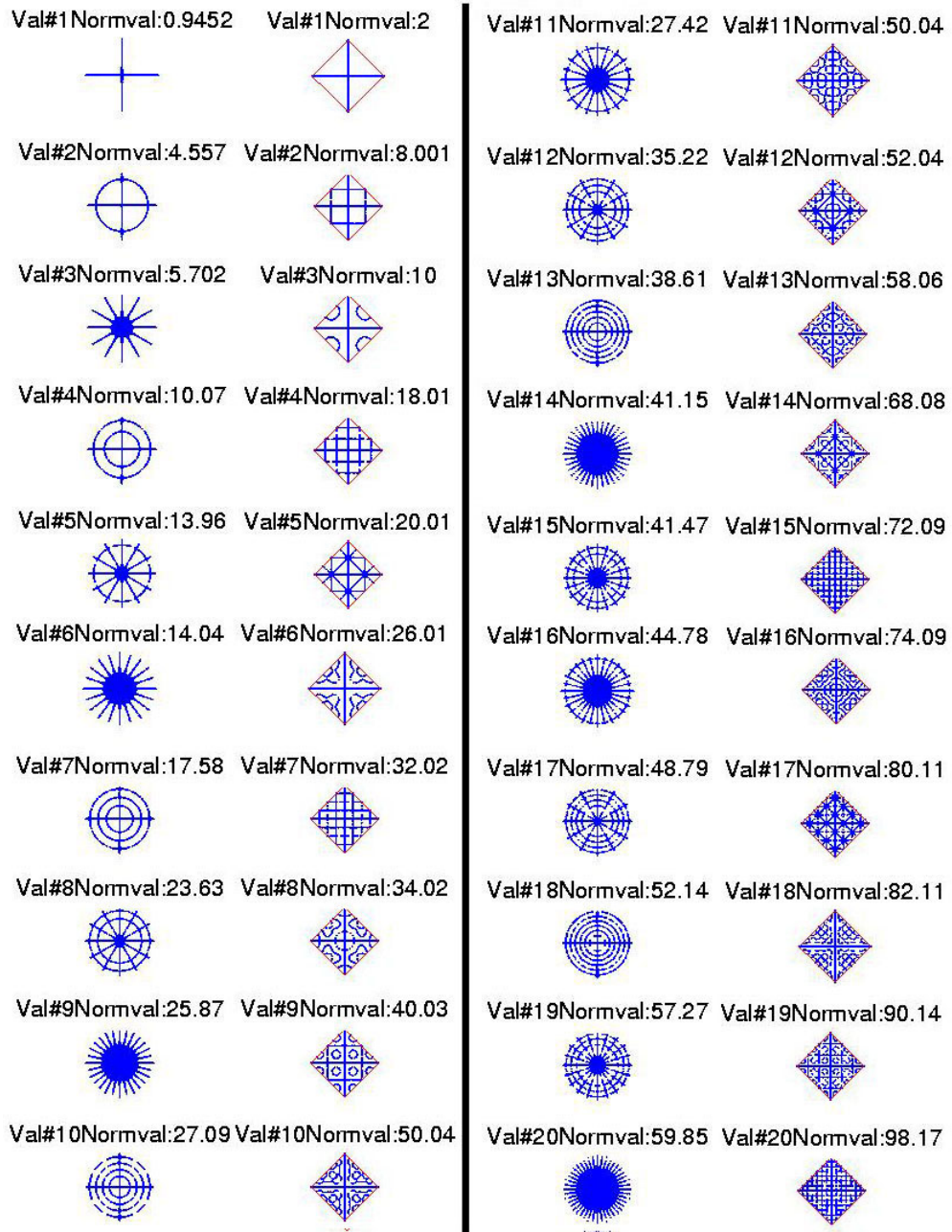


Figure 15: $(1 + -)$ Eigenfunction correspondences

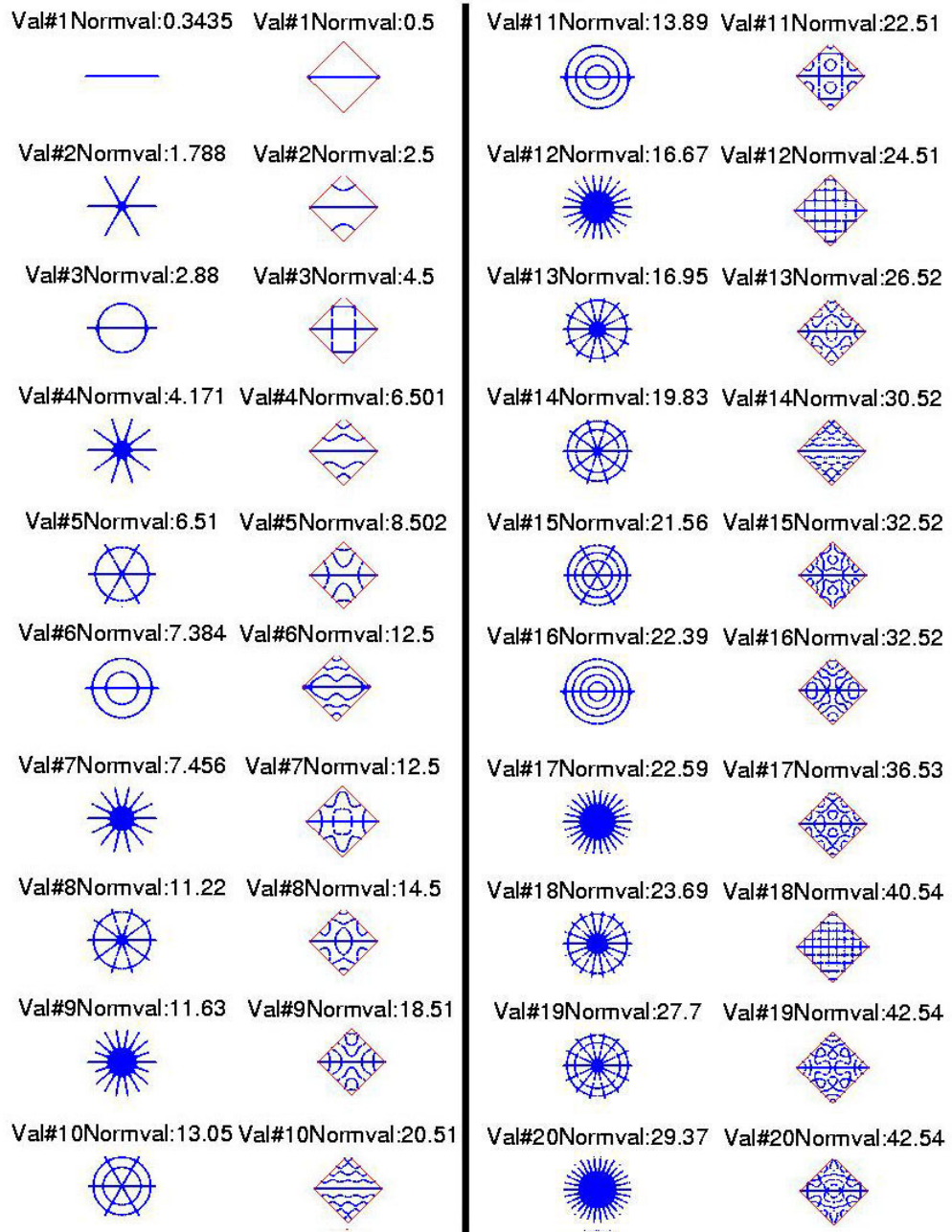


Figure 16: (2) Eigenfunction correspondences

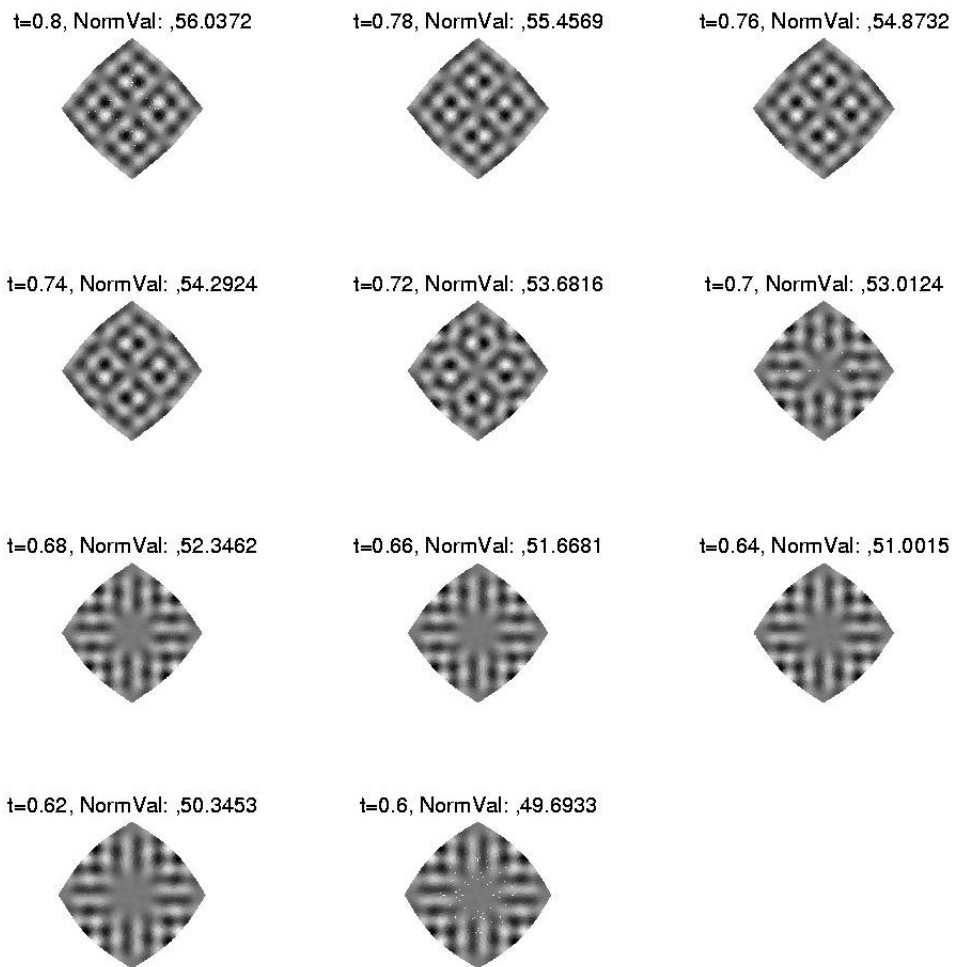


Figure 17: (1 - -) Family Tenth Eigenvalue Zoom

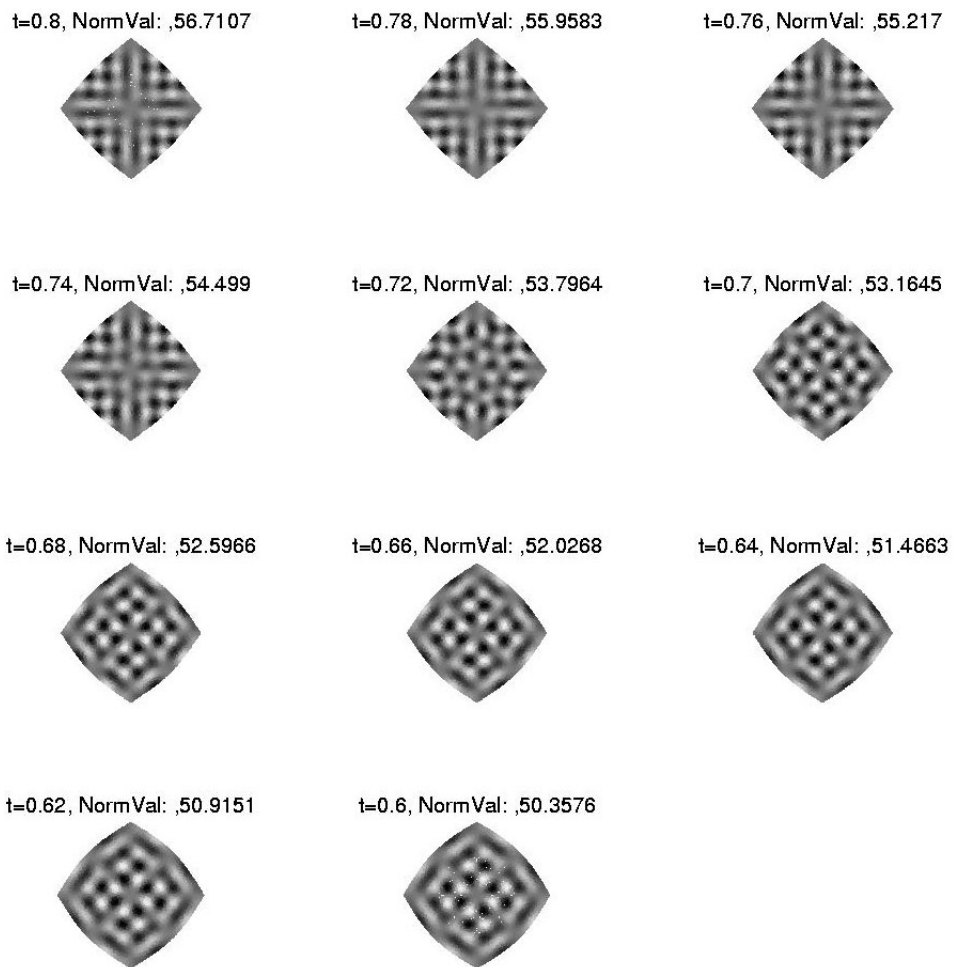


Figure 18: (1 - -) Family Eleventh Eigenvalue Zoom

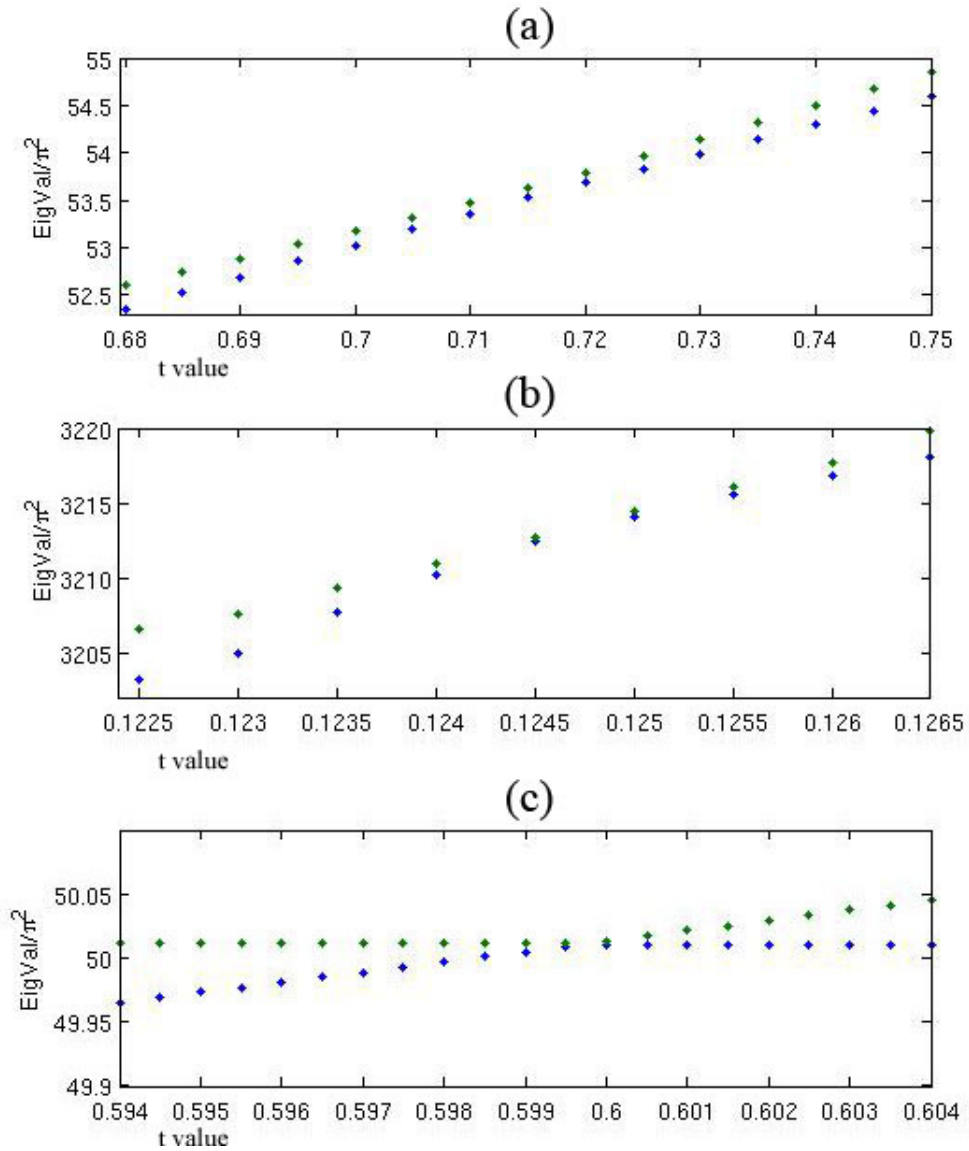


Figure 19: Eigenvalue Dynamics Summary. (a) A *collision*. Tenth and eleventh ($1 - -$) eigenvalues of $H(t, \cdot, \cdot)$ as in Figs. 17 and 18. (b) A *non-crossing tangency*, with (analytically determined) two-dimensional eigenspace. These are two ($1 + +$) eigenvalues of the homotopy $G_0(t, \cdot, \cdot)$ of Section 3 as in Figs. 36 and 37. (c) A *crossing*, with (experimentally determined) two-dimensional eigenspace. These are the sixth and seventh ($1 + -$) eigenvalues of the homotopy $G_0(t, \cdot, \cdot)$ of Section 3 as in Figs. 32 and 33.

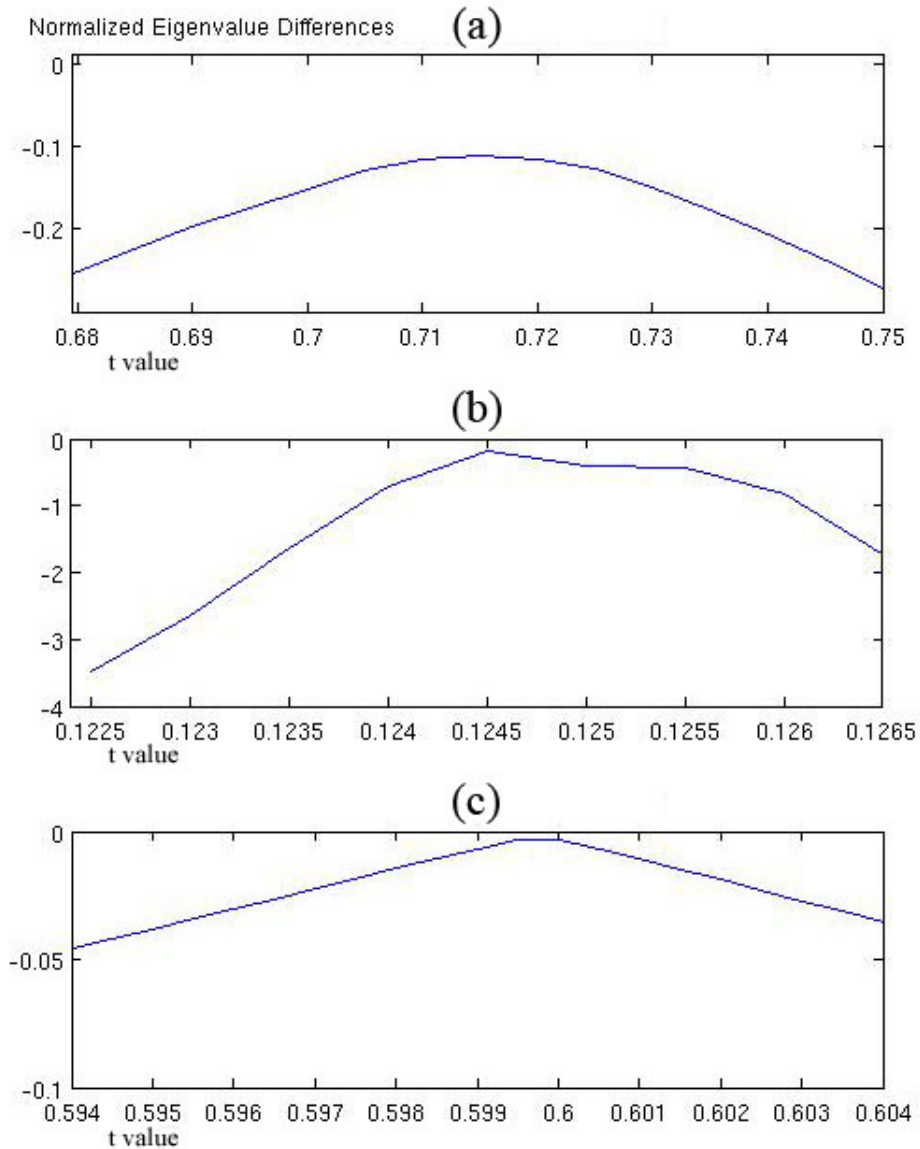


Figure 20: Eigenvalue Dynamics Summary, Eigenvalue Differences $\lambda_{j+1} - \lambda_j$ from Fig. 19. (a) A *collision*. Tenth and eleventh ($1 - -$) eigenvalues of $H(t, \cdot, \cdot)$ as in Figs. 17 and 18. (b) A *non-crossing* tangency, with (analytically determined) two-dimensional eigenspace. These are two ($1 + +$) eigenvalues of the homotopy $G_0(t, \cdot, \cdot)$ of Section 3 as in Figs. 36 and 37. (c) A *crossing*, with (experimentally determined) two-dimensional eigenspace. These are the sixth and seventh ($1 + -$) eigenvalues of the homotopy $G_0(t, \cdot, \cdot)$ of Section 3 as in Figs. 32 and 33.

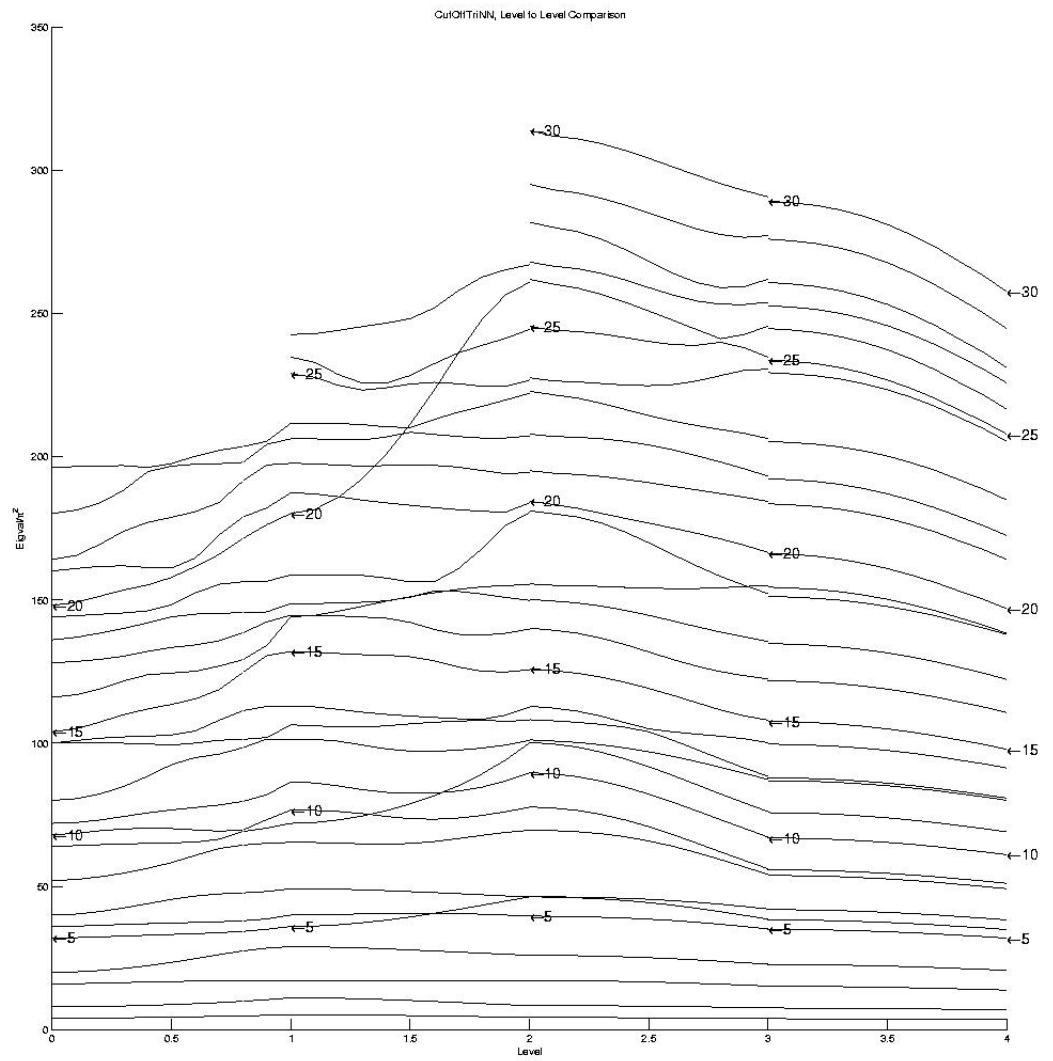


Figure 21: G_0 through G_3 , (1 + +) Eigenvalue Summary Plot

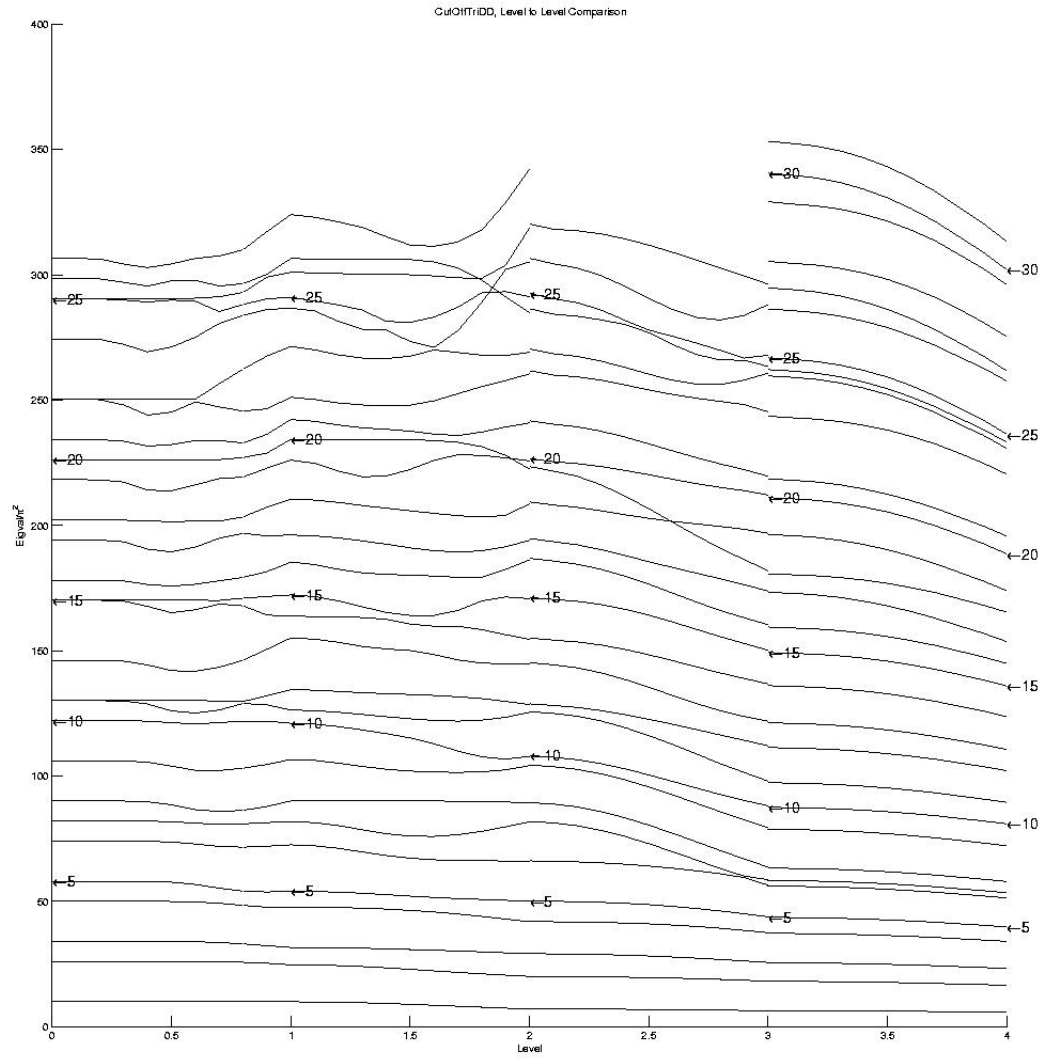


Figure 22: G_0 through G_3 , (1 - -) Eigenvalue Summary Plot

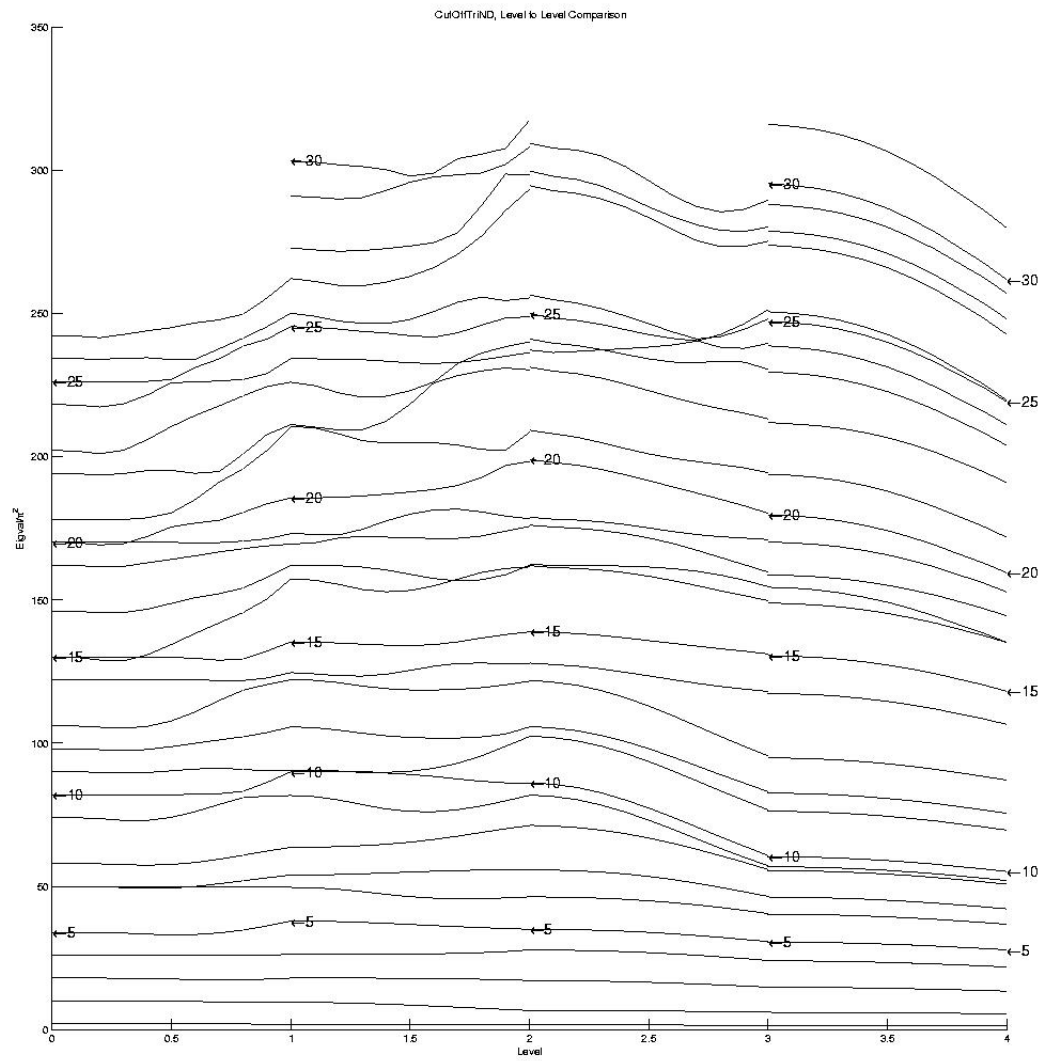


Figure 23: G_0 through G_3 , (1 - +) Eigenvalue Summary Plot

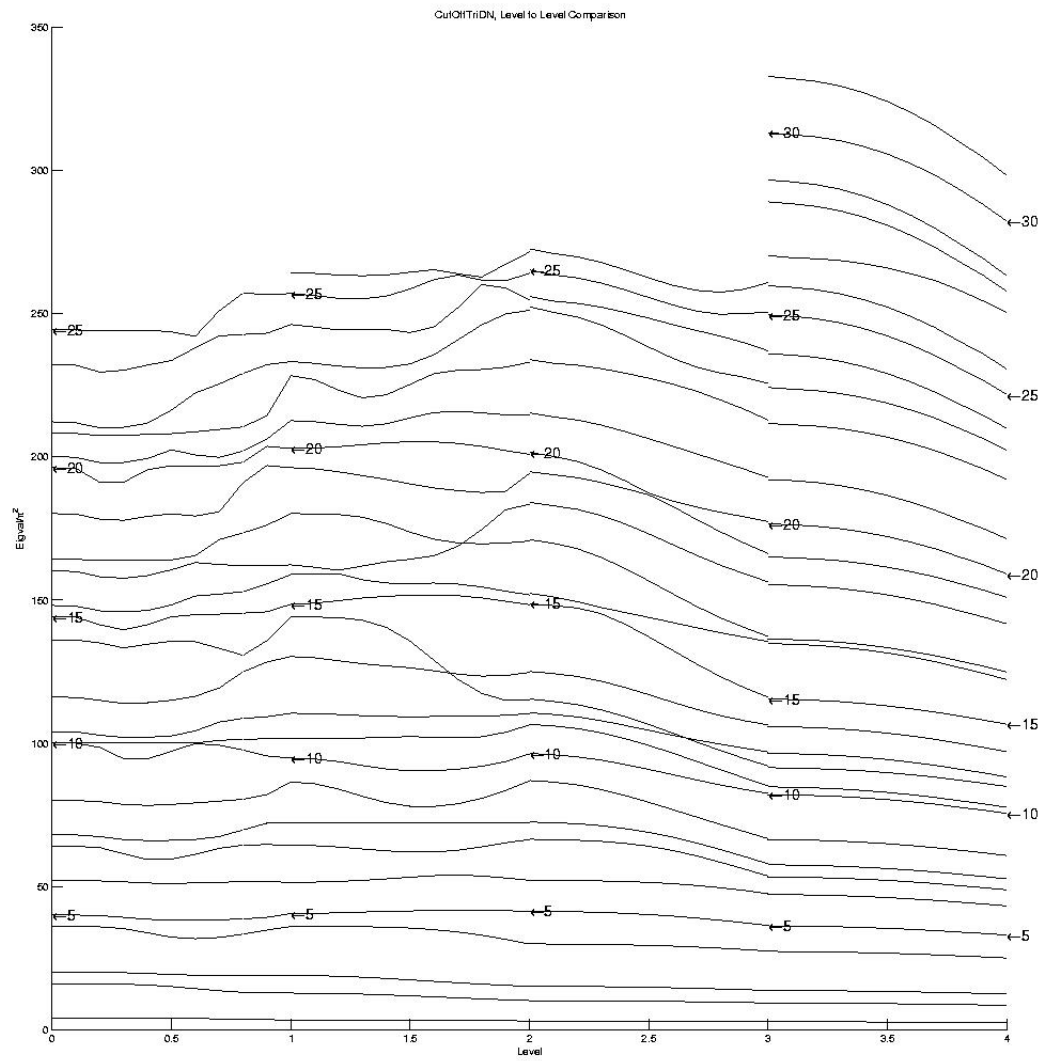


Figure 24: G_0 through G_3 , (1 + -) Eigenvalue Summary Plot

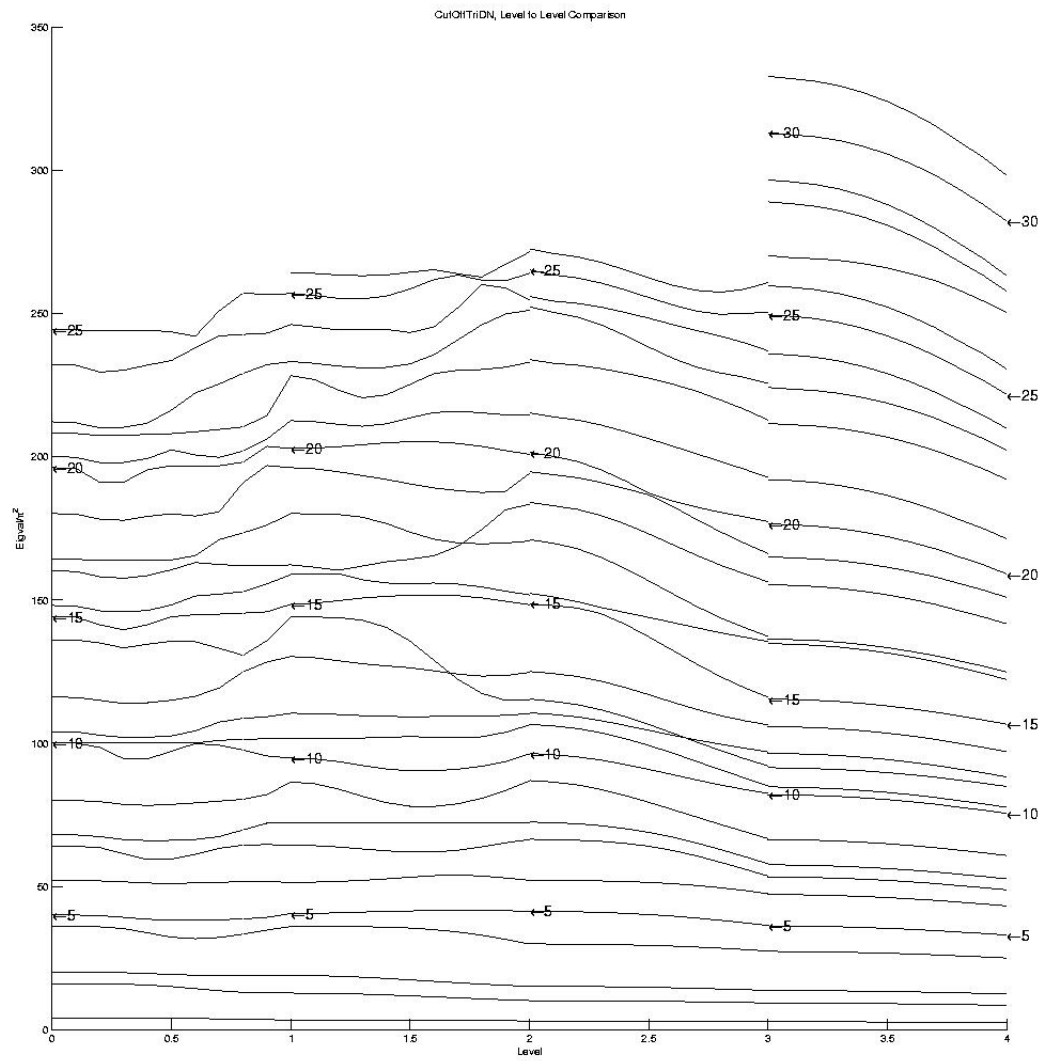
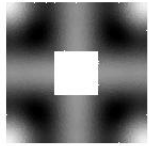


Figure 25: G_0 through G_3 , (2) Eigenvalue Summary Plot

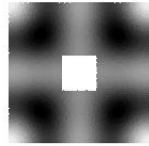
t=0.167, NormVal: ,17.2396



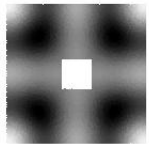
t=0.15, NormVal: ,17.224



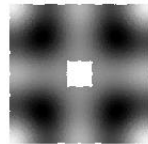
t=0.133, NormVal: ,17.1646



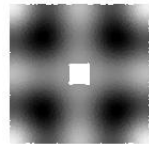
t=0.117, NormVal: ,17.0669



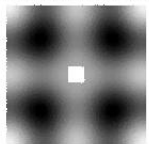
t=0.1, NormVal: ,16.9383



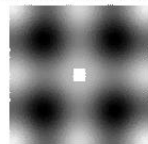
t=0.0833, NormVal: ,16.7846



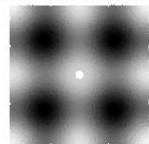
t=0.0667, NormVal: ,16.6091



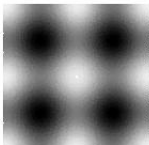
t=0.05, NormVal: ,16.4174



t=0.0333, NormVal: ,16.2246



t=0.0167, NormVal: ,16.0669



t=0, NormVal: ,16.0014

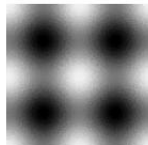


Figure 26: $G_0, (1++)$ EigVal 4 Homotopy

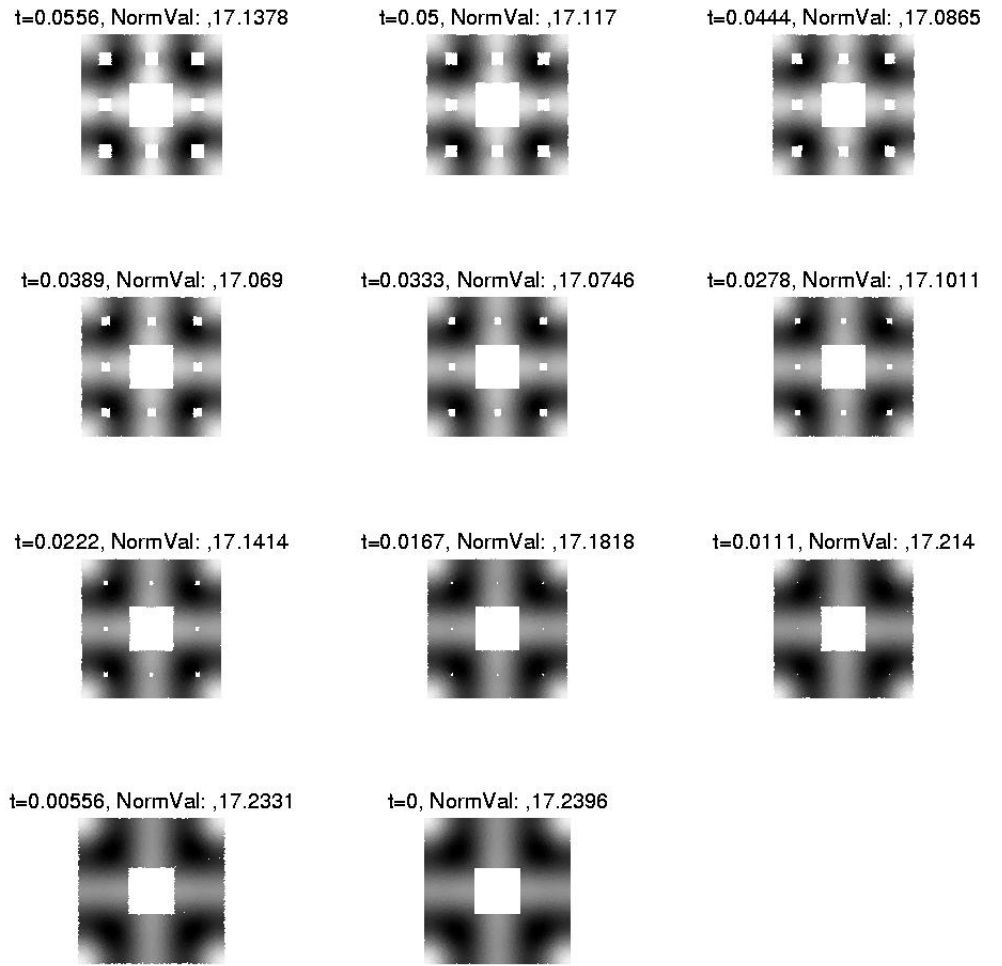


Figure 27: $G_1, (1++)$ EigVal 4 Homotopy

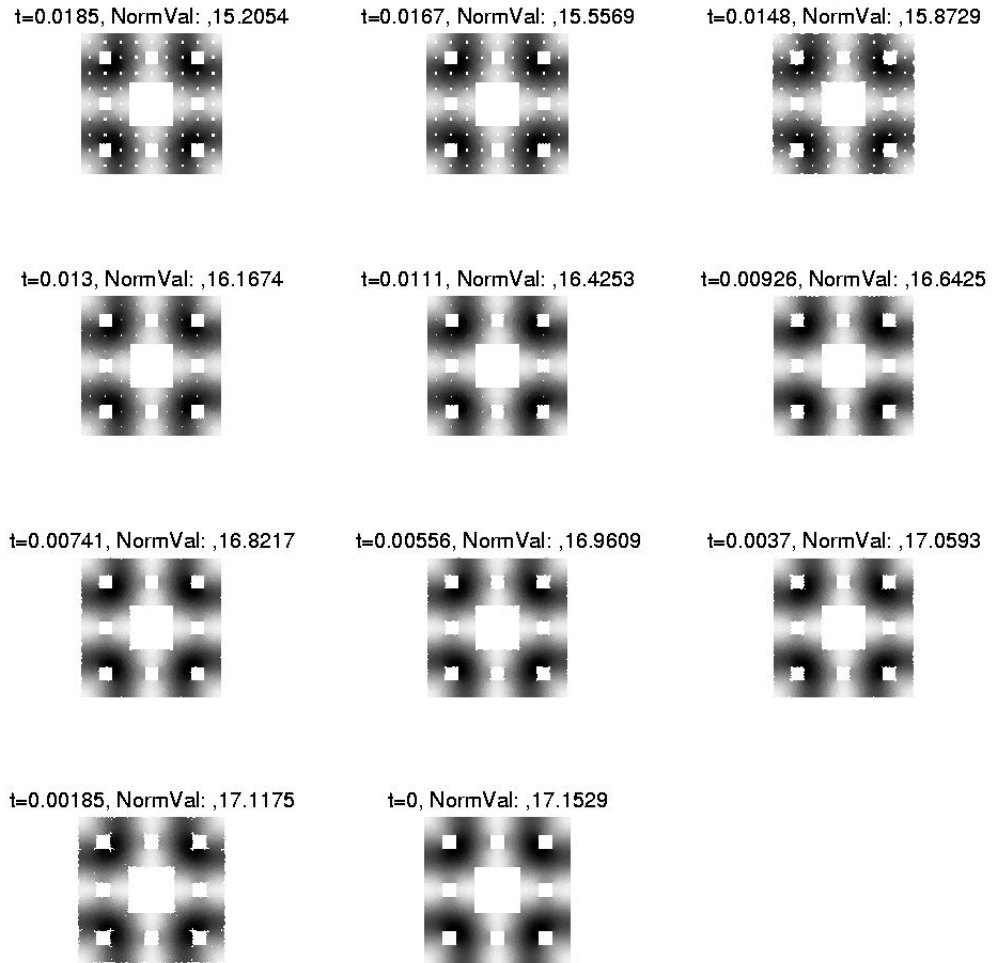
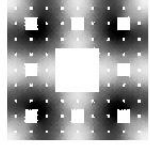


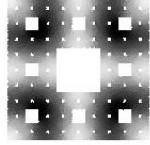
Figure 28: $G_2, (1++)$ EigVal 4 Homotopy

OutOfRange, Eigenfunction Homotopy

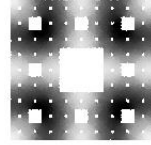
t=0.00617, NormVal: ,13.7955



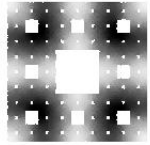
t=0.00556, NormVal: ,14.0301



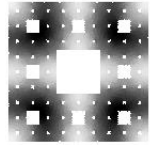
t=0.00494, NormVal: ,14.2315



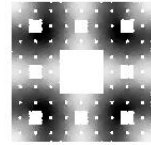
t=0.00432, NormVal: ,14.4429



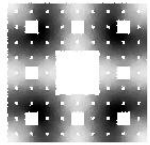
t=0.0037, NormVal: ,14.6164



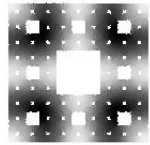
t=0.00309, NormVal: ,14.7727



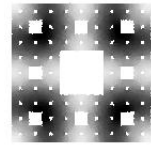
t=0.00247, NormVal: ,14.8994



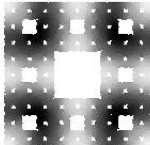
t=0.00185, NormVal: ,15.002



t=0.00123, NormVal: ,15.0731



t=0.000617, NormVal: ,15.116



t=0, NormVal: ,15.1459

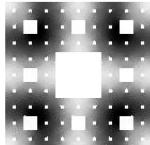
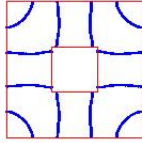
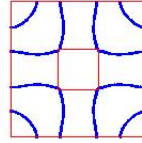


Figure 29: $G_3, (1++)$ EigVal 4 Homotopy

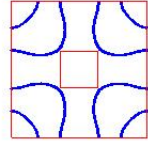
t=0.167, NormVal: ,17.2396



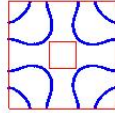
t=0.15, NormVal: ,17.224



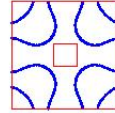
t=0.133, NormVal: ,17.1646



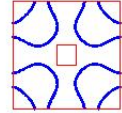
t=0.117, NormVal: ,17.0669



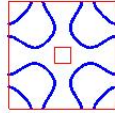
t=0.1, NormVal: ,16.9383



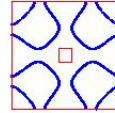
t=0.0833, NormVal: ,16.7846



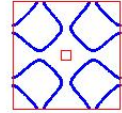
t=0.0667, NormVal: ,16.6091



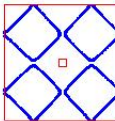
t=0.05, NormVal: ,16.4174



t=0.0333, NormVal: ,16.2246



t=0.0167, NormVal: ,16.0669



t=0, NormVal: ,16.0014

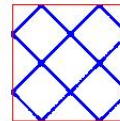


Figure 30: $G_0, (1 + +)$ EigVal 4 Nodal Homotopy

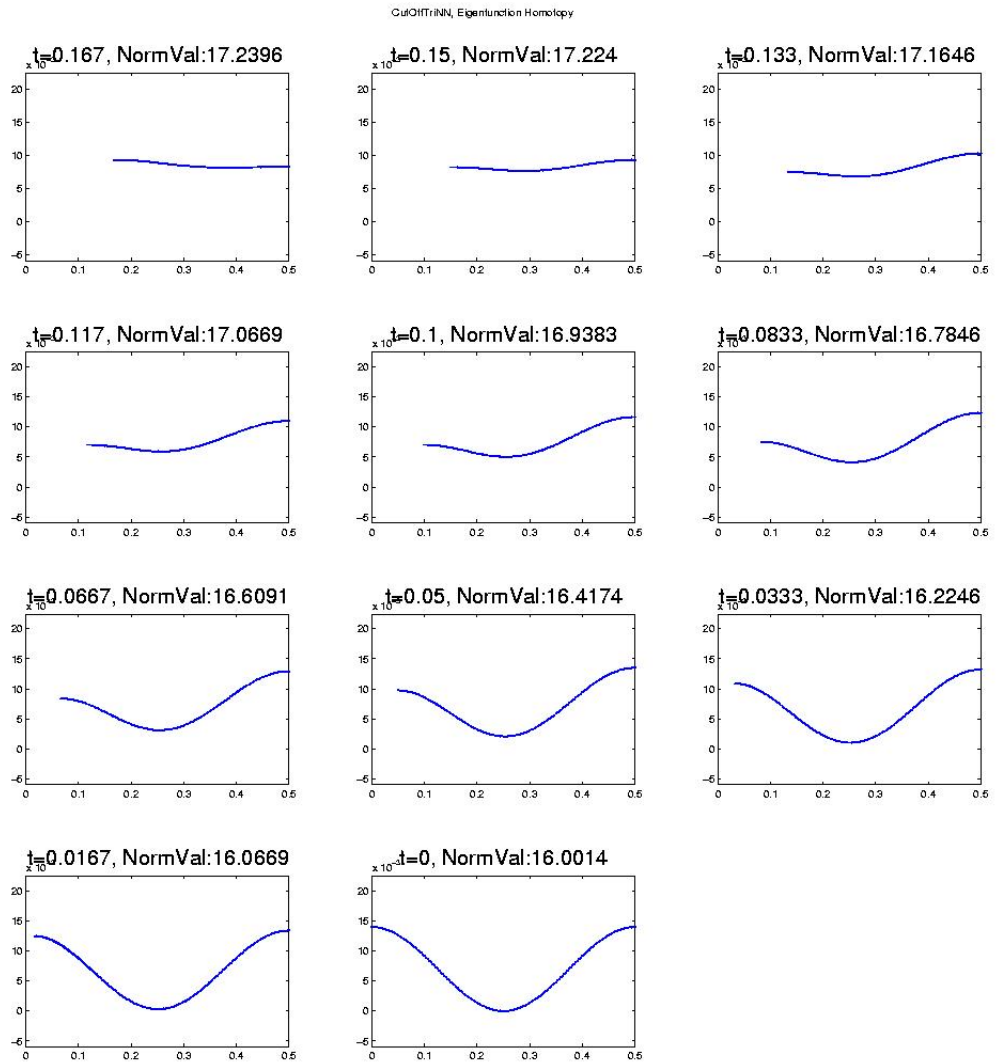


Figure 31: $G_0, (1++)$ EigVal 4 Line Homotopy

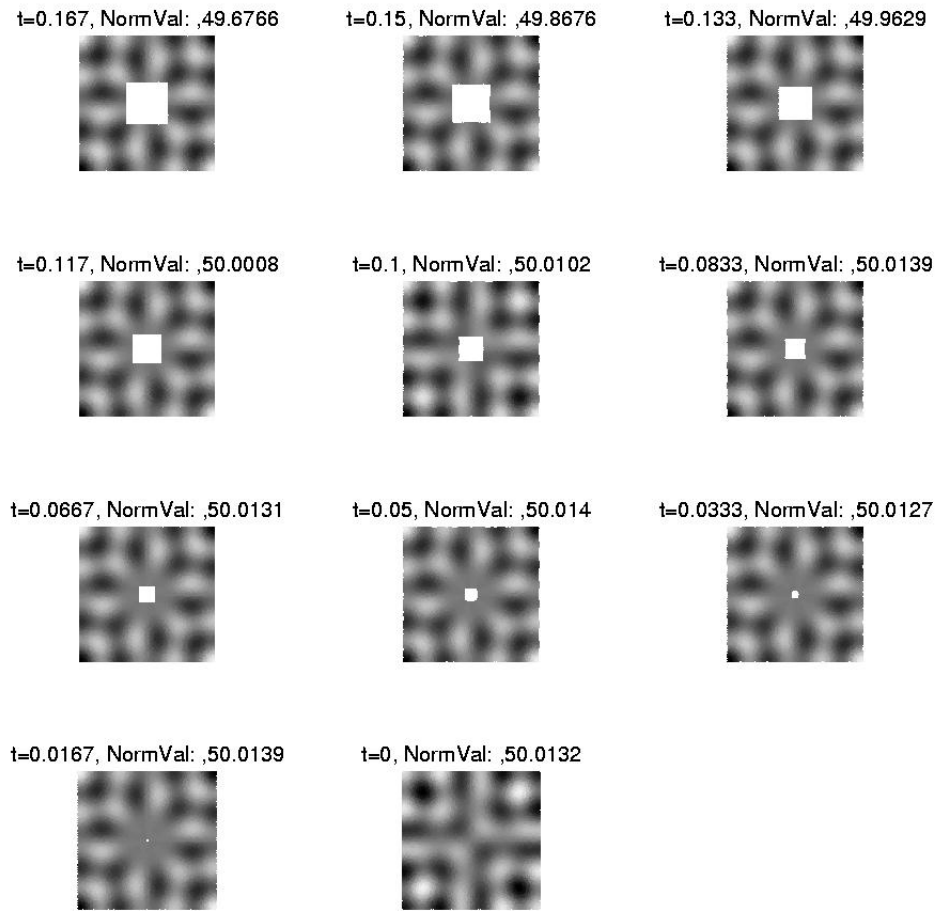


Figure 32: $(1 + -)$ EigVal 6

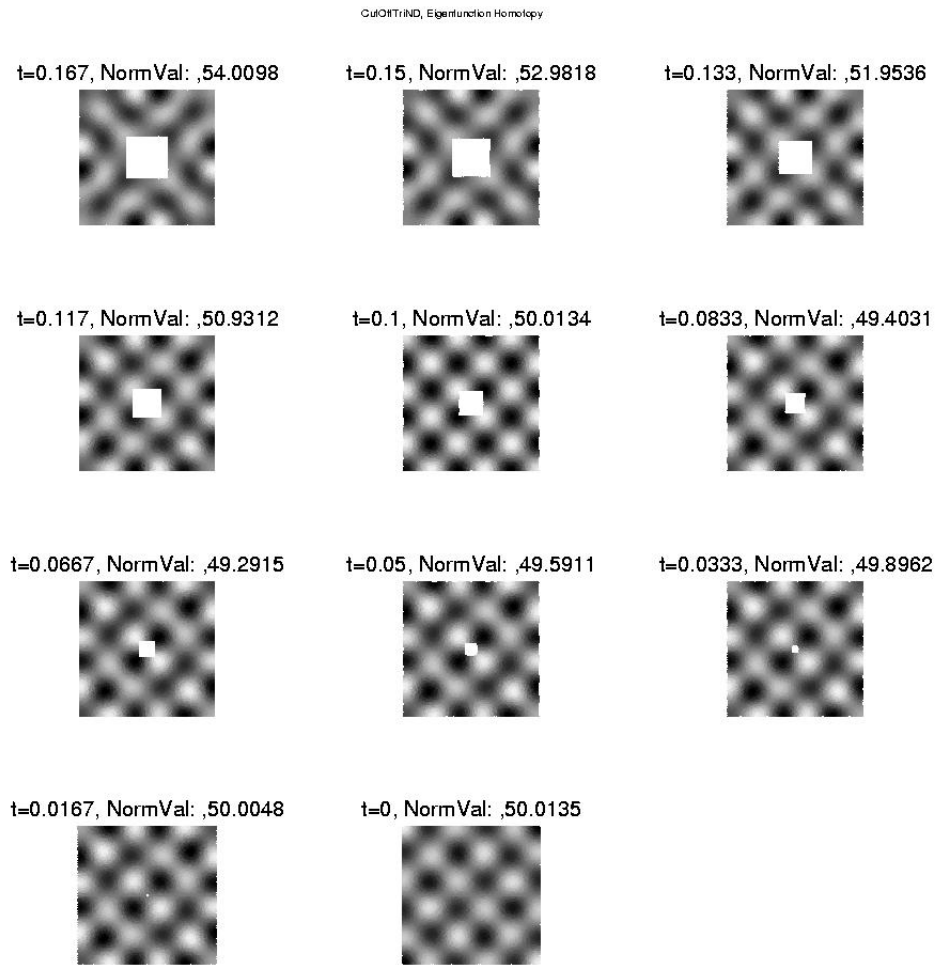
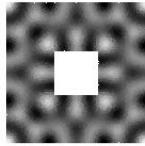
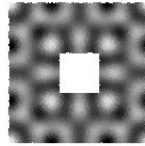


Figure 33: $(1 + -)$ EigVal 7

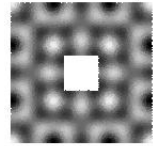
t=0.167, NormVal: ,113.032



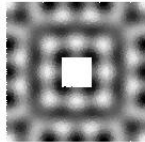
t=0.15, NormVal: ,112.882



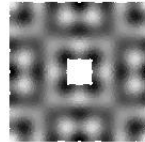
t=0.133, NormVal: ,111.365



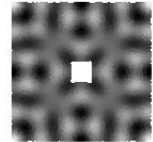
t=0.117, NormVal: ,108.037



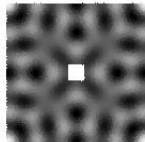
t=0.1, NormVal: ,104.287



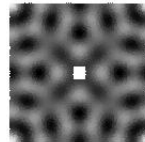
t=0.0833, NormVal: ,102.844



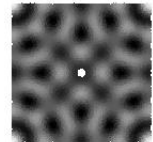
t=0.0667, NormVal: ,102.485



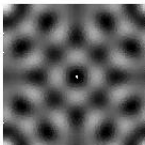
t=0.05, NormVal: ,102.216



t=0.0333, NormVal: ,101.792



t=0.0167, NormVal: ,100.927



t=0, NormVal: ,100.055

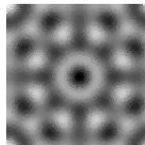
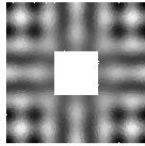
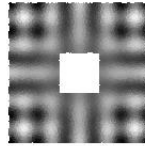


Figure 34: (1 + +) EigVal 13

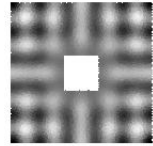
t=0.167, NormVal: ,101.486



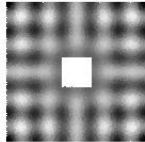
t=0.15, NormVal: ,101.48



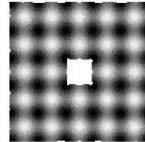
t=0.133, NormVal: ,101.364



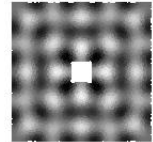
t=0.117, NormVal: ,101.031



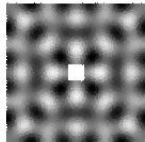
t=0.1, NormVal: ,100.054



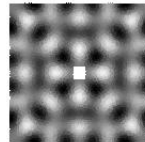
t=0.0833, NormVal: ,99.3288



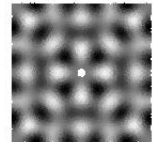
t=0.0667, NormVal: ,99.7791



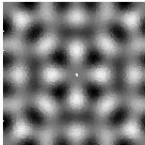
t=0.05, NormVal: ,100.012



t=0.0333, NormVal: ,100.05



t=0.0167, NormVal: ,100.053



t=0, NormVal: ,100.057

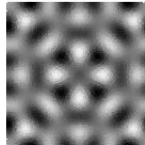


Figure 35: (1 + +) EigVal 14

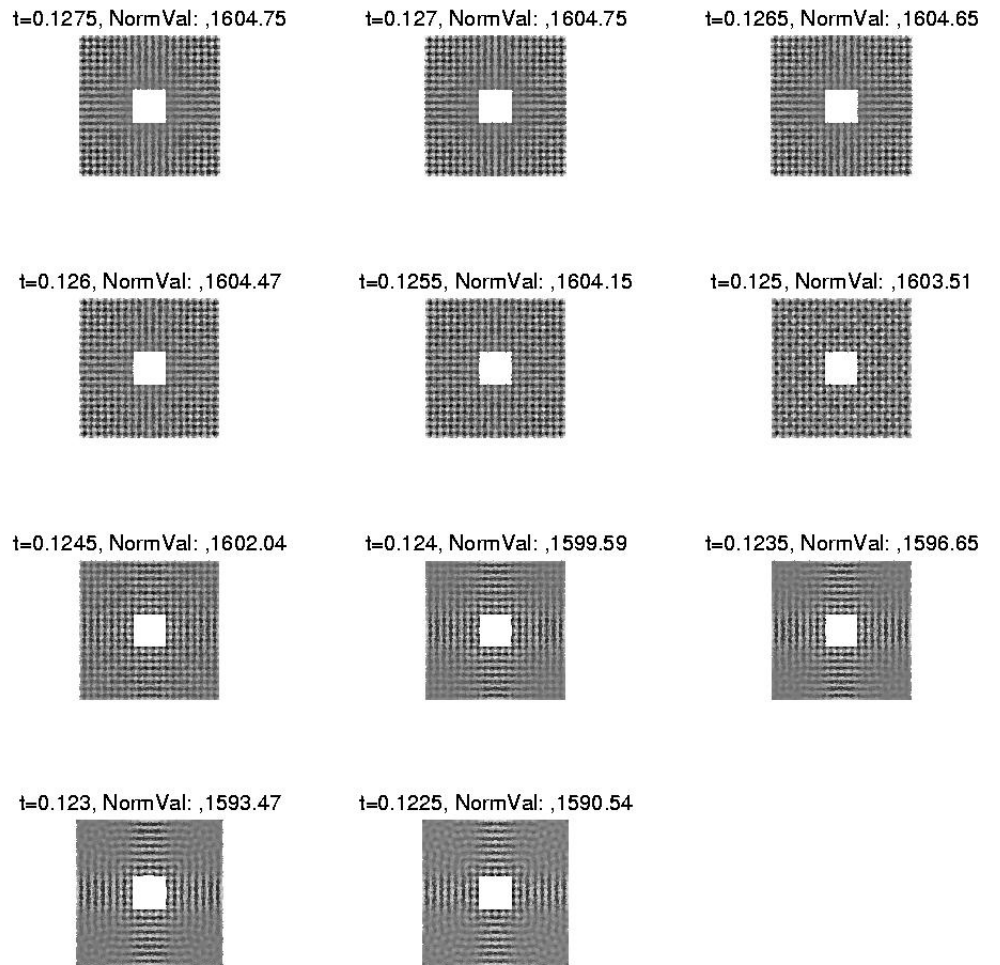


Figure 36: $\lambda = 1600$ at $t = .125$, EigFcn 1

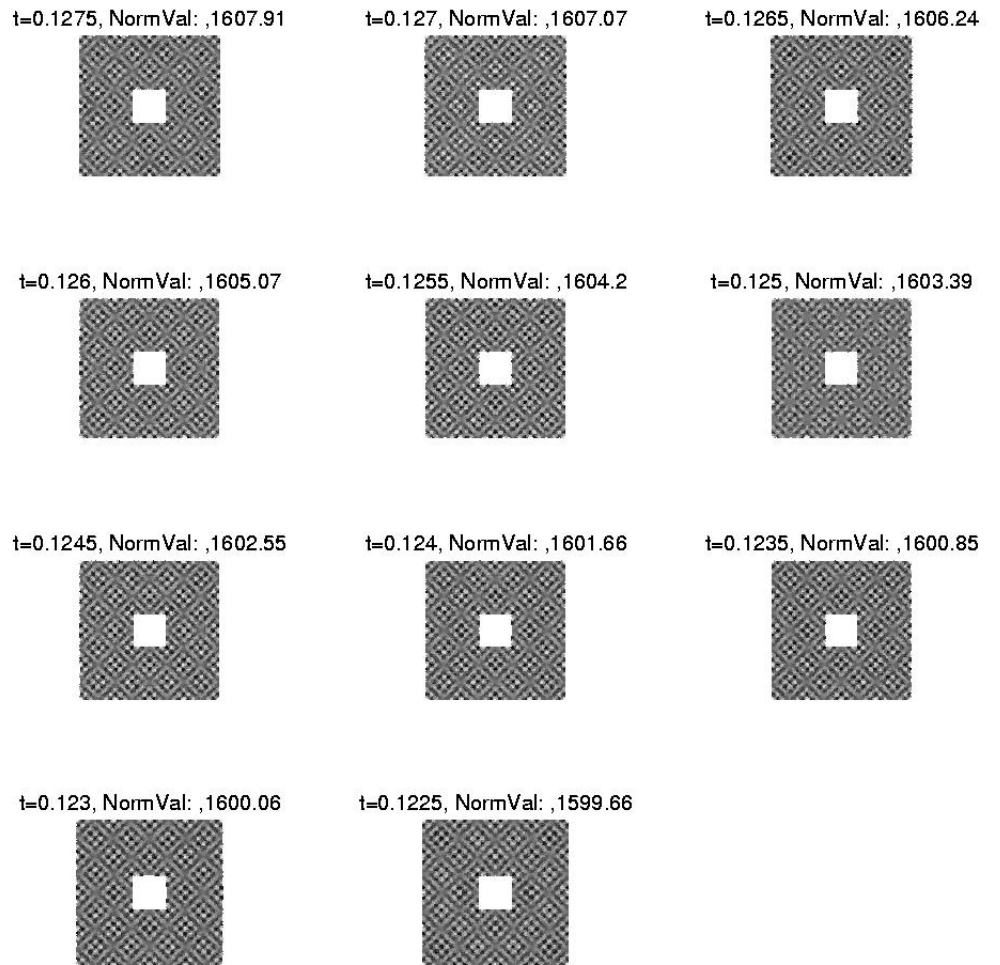


Figure 37: $\lambda = 1600$ at $t = .125$, EigFcn 2